in brack... in Eqs. (3.3.16) and (3.3.17) are thus the *... ...tical deflection and moment amplification factors.*

To simplify the expressions for the maximum deflection equation (3.3.16) and the maximum moment equation (3.3.17), we use the power series expansion for $\tan u$

$$\tan u = u + \frac{1}{3}u^3 + \frac{2}{15}u^5 + \frac{17}{315}u^7 + \cdots \tag{3.3.18}$$

Upon substituting Eq. (3.3.18) into Eqs. (3.3.16) and (3.3.17) and simplifying, it can be shown that these equations can be written approximately as

$$y_{\max} \approx y_0\left[\frac{1}{1-\left(\frac{P}{P_e}\right)}\right] \tag{3.3.19}$$

$$M_{\max} \approx M_0\left[\frac{1-0.18(P/P_e)}{1-(P/P_e)}\right] \approx M_0\left[\frac{1-0.2(P/P_e)}{1-(P/P_e)}\right] \tag{3.3.20}$$

in which the terms in brackets in the above equations are the *design deflection and moment amplification factors,* respectively.

Tables 3.3 and 3.4 show a numerical comparison of the theoretical and design deflection and moment amplification factors, respectively. Good correlation between the theoretical and design amplification factors are observed.

At this point, the reader should recognize the similarity in form of the deflection amplification factors in Eqs. (3.2.35) and (3.3.19) and the

Table 3.3 Theoretical and Design Deflection Amplification Factor for a Beam-Column with a Concentrated Lateral Load at Midspan

$u = \frac{kL}{2} = \frac{\pi}{2}\sqrt{\frac{P}{P_e}}$	Theoretical Eq. (3.3.16)	Design Eq. (3.3.19)
0	1.000	1.000
0.20	1.016	1.016
0.40	1.068	1.069
0.60	1.169	1.171
0.80	1.346	1.350
1.00	1.672	1.681
1.20	2.382	2.402
1.40	4.808	4.863
$\pi/2$	∞	∞

T... 3.4 Theoretical and Design Moment Amplification Factors for a Beam-Column with a Concentrated Lateral Load at Midspan

$u = \frac{kL}{2} = \frac{\pi}{2}\sqrt{\frac{P}{P_e}}$	Theoretical Eq. (3.3.17)	Design Eq. (3.3.20)
0	1.000	1.000
0.20	1.014	1.013
0.40	1.057	1.055
0.60	1.140	1.137
0.80	1.287	1.280
1.00	1.557	1.545
1.20	2.143	2.122
1.40	4.141	4.090
$\pi/2$	∞	∞

W.F. Chen & E.M. Lui "Structural Stability" - Elsevier -

similarity in form of the moment amplification factors in Eqs. (3.2.41) and (3.3.20) for the simply supported beam-column under uniformly distributed and midspan concentrated lateral loads. We shall take advantage of these similarities in developing design formulas for beam-columns. This will be discussed later.

3.4 BEAM-COLUMNS SUBJECTED TO END MOMENTS

3.4.1 The Closed-Form Solution (Fig. 3.4)

So far, we have considered only the cases in which the primary bending moments in the beam-columns are caused by in-span lateral loads. In this section, we shall consider the case in which the primary bending moment is caused by end moments in the beam-column. Shown in Fig. 3.4a is a beam-column acted on by end couples M_A and M_B at the left and right ends of the member, respectively, and acted on by an axial force P. Using the free-body diagram of a segment of beam-column of length x from the left end (Fig. 3.4b), the external moment acting on the cut section is

$$M_{ext} = M_A + Py - \frac{M_A + M_B}{L}x \tag{3.4.1}$$

Equating this to the internal moment of $-EIy''$ and rearranging, we have

$$EIy'' + Py = \frac{M_A + M_B}{L}x - M_A \tag{3.4.2}$$

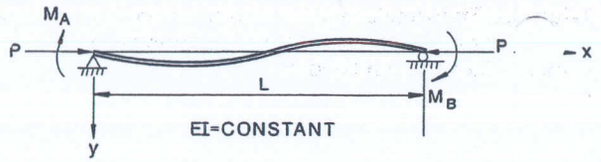

(a)

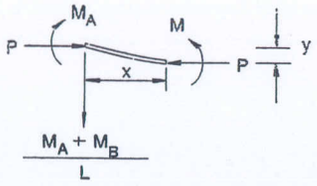

(b)

FIGURE 3.4 Beam-column with end couples (double-curvature bending)

or, using $k^2 = P/EI$, we can write

$$y'' + k^2 y = \frac{M_A + M_B}{LEI} x - \frac{M_A}{EI} \tag{3.4.3}$$

The general solution is

$$y = A \sin kx + B \cos kx + \frac{M_A + M_B}{LEIk^2} x - \frac{M_A}{EIk^2} \tag{3.4.4}$$

The constants A and B can be evaluated by using the boundary conditions

$$y(0) = 0, \qquad y(L) = 0 \tag{3.4.5}$$

From the first boundary condition, we obtain

$$B = \frac{M_A}{EIk^2} \tag{3.4.6}$$

and from the second boundary condition, we obtain

$$A = -\frac{1}{EIk^2 \sin kL}(M_A \cos kL + M_B) \tag{3.4.7}$$

Therefore, Eq. (3.4.4) can now be written as

$$y = -\frac{(M_A \cos kL + M_B)}{EIk^2 \sin kL} \sin kx + \frac{M_A}{EIk^2} \cos kx + \frac{M_A + M_B}{LEIk^2} x - \frac{M_A}{EIk^2} \tag{3.4.8}$$

from which

$$y' = -\frac{(M_A \cos kL + M_B)}{EIk \sin kL} \cos kx - \frac{M_A}{EIk} \sin kx + \frac{M_A + M_B}{LEIk^2} \tag{3.4.9}$$

and

$$y'' = \frac{(M_A \cos kL + M_B)}{EI \sin kL} \sin kx - \frac{M_A}{EI} \cos kx \tag{3.4.10}$$

and

$$y''' = \frac{k(M_A \cos kL + M_B)}{EI \sin kL} \cos kx + \frac{kM_A}{EI} \sin kx \tag{3.4.11}$$

To determine the location of the maximum moment, we set the shear force ($-EIy'''$), or Eq. (3.4.11), equal to zero. In doing so, we obtain the location $\bar{x}$

$$\tan k\bar{x} = \frac{-(M_A \cos kL + M_B)}{M_A \sin kL} \tag{3.4.12}$$

From Fig. 3.5, it can be seen that

$$\sin k\bar{x} = \frac{(M_A \cos kL + M_B)}{\sqrt{M_A^2 + 2M_A M_B \cos kL + M_B^2}} \tag{3.4.13}$$

$$\cos k\bar{x} = \frac{-M_A \sin kL}{\sqrt{M_A^2 + 2M_A M_B \cos kL + M_B^2}} \tag{3.4.14}$$

FIGURE 3.5 Trigonometric relationship

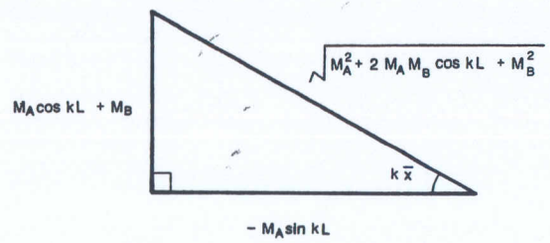

Table 3.6 Theoretical and Design Moment Amplification Factors for a Fixed-Ended Beam-Column Loaded by a Uniformly Distributed Lateral Load

$u=\frac{kL}{2}=\frac{\pi}{2K}\sqrt{\frac{P}{P_{ek}}}$	Theoretical Eq. (3.6.31)	Design Eq. (3.6.19)
0	0	0
0.20	1.003	1.002
0.40	1.011	1.010
0.60	1.025	1.023
0.80	1.045	1.042
1.00	1.074	1.068
1.20	1.111	1.102
1.40	1.161	1.149
π	∞	∞

Eq. (3.6.19), M_0 is now $wL^2/12$, $P_{ek}=\pi^2EI/(KL)^2$ where $K=0.5$. The value of Ψ is

$$\Psi=\frac{1}{(P/P_{ek})}\left\{\left|\frac{3(\tan u-u)}{u^2\tan u}\right|[1-(P/P_{ek})]-1\right\} \tag{3.6.32}$$

Again, the value of Ψ does not vary too much for various values of P/P_{ek}. By choosing a Ψ-value equal to -0.4, we will observe a good correlation between the theoretical M_{max} as expressed in Eq. (3.6.31) and the approximate M_{max} as expressed in Eq. (3.6.19) (Table 3.6).

3.7 SLOPE-DEFLECTION EQUATIONS

In this section, we will develop the *slope-deflection equations* for a beam-column. Consider the beam-column shown in Fig. 3.17; we now want to establish a relationship between the end moments (M_A, M_B) and the end rotations (θ_A, θ_B).

From Eq. (3.4.8), the deflection function for this beam-column has the

FIGURE 3.17 Beam-column subjected to end moments (without relative joint translation)

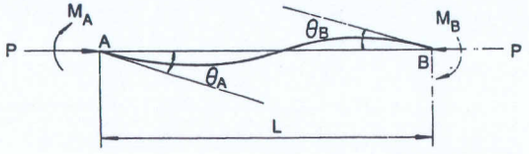

form

$$y=-\frac{(M_A\cos kL+M_B)}{EIk^2\sin kL}\sin kx+\frac{M_A}{EIk^2}\cos kx+\frac{M_A+M_B}{LEIk^2}x-\frac{M_A}{EIk^2} \tag{3.7.1}$$

Rearranging, we have

$$y=-\frac{1}{EIk^2}\left[\frac{\cos kL}{\sin kL}\sin kx-\cos kx-\frac{x}{L}+1\right]M_A-\frac{1}{EIk^2}\left[\frac{1}{\sin kL}\sin kx-\frac{x}{L}\right]M_B \tag{3.7.2}$$

from which

$$y'=-\frac{1}{EIk}\left[\frac{\cos kL}{\sin kL}\cos kx+\sin kx-\frac{1}{kL}\right]M_A-\frac{1}{EIk}\left[\frac{\cos kx}{\sin kL}-\frac{1}{kL}\right]M_B \tag{3.7.3}$$

Using Eq. (3.7.3), the end rotations θ_A and θ_B can be obtained as

$$\theta_A=y'(0)=-\frac{1}{EIk}\left[\frac{\cos kL}{\sin kL}-\frac{1}{kL}\right]M_A-\frac{1}{EIk}\left[\frac{1}{\sin kL}-\frac{1}{kL}\right]M_B=\frac{L}{EI}\left[\frac{\sin kL-kL\cos kL}{(kL)^2\sin kL}\right]M_A+\frac{L}{EI}\left[\frac{\sin kL-kL}{(kL)^2\sin kL}\right]M_B \tag{3.7.4}$$

$$\theta_B=y'(L)=-\frac{1}{EIk}\left[\frac{1}{\sin kL}-\frac{1}{kL}\right]M_A-\frac{1}{EIk}\left[\frac{\cos kL}{\sin kL}-\frac{1}{kL}\right]M_B=\frac{L}{EI}\left[\frac{\sin kL-kL}{(kL)^2\sin kL}\right]M_A+\frac{L}{EI}\left[\frac{\sin kL-kL\cos kL}{(kL)^2\sin kL}\right]M_B \tag{3.7.5}$$

Equations (3.7.4) and (3.7.5) can be written in matrix form as

$$\begin{bmatrix}\theta_A\\ \theta_B\end{bmatrix}=\begin{bmatrix}f_{11} & f_{12}\\ f_{21} & f_{22}\end{bmatrix}\begin{bmatrix}M_A\\ M_B\end{bmatrix} \tag{3.7.6}$$

where

$$f_{11}=f_{22}=\frac{L}{EI}\left[\frac{\sin kL-kL\cos kL}{(kL)^2\sin kL}\right] \tag{3.7.7}$$

$$f_{12}=f_{21}=\frac{L}{EI}\left[\frac{\sin kL-kL}{(kL)^2\sin kL}\right] \tag{3.7.8}$$

From Eq. (3.7.6), we can write

$$\begin{bmatrix}M_A\\ M_B\end{bmatrix}=\begin{bmatrix}f_{11} & f_{12}\\ f_{21} & f_{22}\end{bmatrix}^{-1}\begin{bmatrix}\theta_A\\ \theta_B\end{bmatrix} \tag{3.7.9}$$

or

$$\begin{bmatrix}M_A\\ M_B\end{bmatrix}=\begin{bmatrix}c_{11} & c_{12}\\ c_{21} & c_{22}\end{bmatrix}\begin{bmatrix}\theta_A\\ \theta_B\end{bmatrix} \tag{3.7.10}$$

where

$$c_{11}=c_{22}=\frac{EI}{L}\left[\frac{kL\sin kL-(kL)^2\cos kL}{2-2\cos kL-kL\sin kL}\right] \tag{3.7.11}$$

$$c_{12}=c_{21}=\frac{EI}{L}\left[\frac{(kL)^2-kL\sin kL}{2-2\cos kL-kL\sin kL}\right] \tag{3.7.12}$$

Equation (3.7.10) can be written in its expanded form as

$$M_A=\frac{EI}{L}(s_{ii}\theta_A+s_{ij}\theta_B) \tag{3.7.13}$$

$$M_B=\frac{EI}{L}(s_{ji}\theta_A+s_{jj}\theta_B) \tag{3.7.14}$$

where

$$s_{ii}=s_{jj}=\frac{c_{11}L}{EI}=\frac{c_{22}L}{EI} \tag{3.7.15}$$

$$s_{ij}=s_{ji}=\frac{c_{12}L}{EI}=\frac{c_{21}L}{EI} \tag{3.7.16}$$

are referred to as the *stability functions*.

Equations (3.7.13) and (3.7.14) are the slope-deflection equations for a

Table 3.7 Stability Functions ($kL=\pi\sqrt{P/P_e}$)

		compression		tension	
kL	P/P_e	s_{ii}	s_{ij}	s_{ii}	s_{ij}
0.	0.	4. 0000	2. 0000	4. 0000	2. 0000
0. 0500	0. 0003	3. 9997	2. 0001	4. 0003	1. 9999
0. 1000	0. 0010	3. 9987	2. 0003	4. 0013	1. 9997
0. 1500	0. 0023	3. 9970	2. 0008	4. 0030	1. 9993
0. 2000	0. 0041	3. 9947	2. 0013	4. 0053	1. 9987
0. 2500	0. 0063	3. 9917	2. 0021	4. 0083	1. 9979
0. 3000	0. 0091	3. 9876	2. 0028	4. 0120	1. 9970
0. 3500	0. 0124	3. 9833	2. 0039	4. 0157	1. 9956
0. 4000	0. 0162	3. 9786	2. 0054	4. 0211	1. 9946
0. 4500	0. 0205	3. 9729	2. 0068	4. 0268	1. 9932
0. 5000	0. 0253	3. 9665	2. 0084	4. 0332	1. 9917
0. 5500	0. 0306	3. 9595	2. 0102	4. 0401	1. 9900
0. 6000	0. 0365	3. 9517	2. 0121	4. 0477	1. 9881
0. 6500	0. 0428	3. 9433	2. 0143	4. 0560	1. 9861
0. 7000	0. 0496	3. 9342	2. 0166	4. 0649	1. 9839
0. 7500	0. 0570	3. 9244	2. 0191	4. 0744	1. 9816
0. 8000	0. 0648	3. 9139	2. 0218	4. 0846	1. 9791
0. 8500	0. 0732	3. 9027	2. 0246	4. 0954	1. 9764
0. 9000	0. 0821	3. 8908	2. 0277	4. 1069	1. 9737
0. 9500	0. 0914	3. 8782	2. 0309	4. 1189	1. 9707
1. 0000	0. 1013	3. 8649	2. 0344	4. 1316	1. 9677
1. 0500	0. 1117	3. 8508	2. 0380	4. 1449	1. 9645
1. 1000	0. 1226	3. 8360	2. 0419	4. 1588	1. 9611
1. 1500	0. 1340	3. 8205	2. 0460	4. 1734	1. 9577
1. 2000	0. 1459	3. 8043	2. 0502	4. 1885	1. 9541
1. 2500	0. 1583	3. 7873	2. 0547	4. 2042	1. 9503
1. 3000	0. 1712	3. 7695	2. 0594	4. 2205	1. 9465
1. 3500	0. 1847	3. 7510	2. 0644	4. 2374	1. 9425
1. 4000	0. 1986	3. 7317	2. 0695	4. 2549	1. 9384
1. 4500	0. 2130	3. 7116	2. 0749	4. 2729	1. 9342
1. 5000	0. 2280	3. 6907	2. 0806	4. 2916	1. 9299
1. 5500	0. 2434	3. 6690	2. 0865	4. 3107	1. 9255
1. 6000	0. 2594	3. 6466	2. 0926	4. 3305	1. 9210
1. 6500	0. 2758	3. 6233	2. 0990	4. 3508	1. 9163
1. 7000	0. 2928	3. 5991	2. 1057	4. 3716	1. 9116
1. 7500	0. 3103	3. 5741	2. 1127	4. 3929	1. 9068
1. 8000	0. 3283	3. 5483	2. 1199	4. 4148	1. 9019
1 8500	0. 3468	3. 5216	2. 1275	4. 4373	1. 8969
1. 9000	0. 3658	3. 4940	2. 1353	4. 4602	1. 8919
1. 9500	0. 3853	3. 4655	2. 1434	4. 4836	1. 8867
2. 0000	0. 4053	3. 4361	2. 1519	4. 5076	1. 8815
2. 0500	0. 4258	3. 4058	2. 1607	4. 5320	1. 8762
2. 1000	0. 4468	3. 3745	2. 1699	4. 5569	1. 8708
2. 1500	0. 4684	3. 3422	2. 1794	4. 5823	1. 8654
2. 2000	0. 4904	3. 3090	2. 1893	4. 6082	1. 8599
2. 2500	0. 5129	3. 2748	2. 1996	4. 6345	1. 8544
2. 3000	0. 5360	3. 2395	2. 2102	4. 6613	1. 8488

(continued)

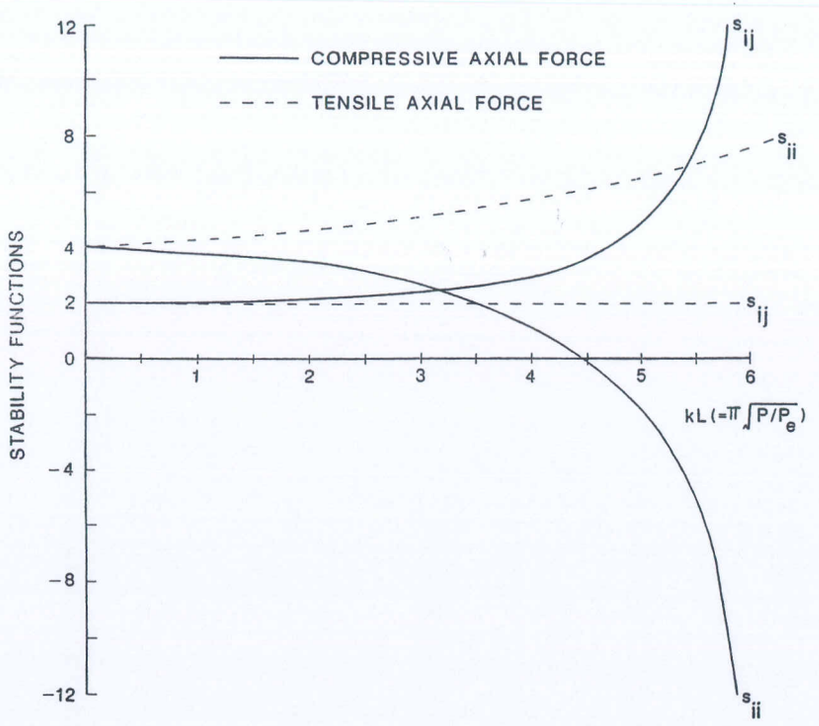

FIGURE 3.18 Plot of stability functions

1. The beam is prismatic.
2. There is no relative joint displacement between the two ends of the member, i.e., the member does not sway.
3. The member is continuous, i.e., there is no internal hinge or discontinuity in the member.
4. There is no in-span transverse loadings on the member.
5. The axial force in the member is compressive.

If these conditions are not satisfied, modifications to the slope-deflection equations are necessary. Some of these modifications to special cases of beam-columns are described below.

3.8.1 Member with Sway

If there is a relative joint translation between the member ends, designated as Δ in Fig. 3.19, the slope-deflection equations are modified

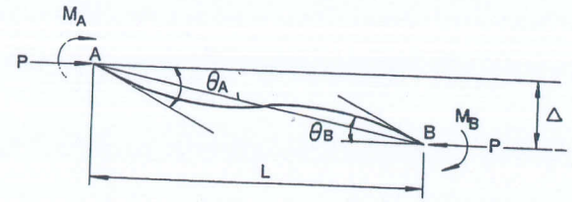

FIGURE 3.19 Beam-column subjected to end moments (with relative joint translation)

as

$$M_A = \frac{EI}{L}\left[s_{ii}\left(\theta_A - \frac{\Delta}{L}\right) + s_{ij}\left(\theta_B - \frac{\Delta}{L}\right)\right]$$

$$= \frac{EI}{L}\left[s_{ii}\theta_A + s_{ij}\theta_B - (s_{ii} + s_{ij})\frac{\Delta}{L}\right] \qquad (3.8.1)$$

$$M_B = \frac{EI}{L}\left[s_{ij}\left(\theta_A - \frac{\Delta}{L}\right) + s_{ii}\left(\theta_B - \frac{\Delta}{L}\right)\right]$$

$$= \frac{EI}{L}\left[s_{ij}\theta_A + s_{ii}\theta_B - (s_{ii} + s_{ij})\frac{\Delta}{L}\right] \qquad (3.8.2)$$

3.8.2 Member with a Hinge at One End

If a hinge is present at one end of the member—as in Fig. 3.20a, in which the B end is hinged—the moment there is zero, i.e.,

$$M_B = \frac{EI}{L}(s_{ij}\theta_A + s_{ii}\theta_B) = 0 \qquad (3.8.3)$$

from which

$$\theta_B = -\frac{s_{ij}}{s_{ii}}\theta_A \qquad (3.8.4)$$

Upon substituting Eq. (3.8.4) into Eq. (3.7.13), we have

$$M_A = \frac{EI}{L}\left(s_{ii} - \frac{s_{ij}^2}{s_{ii}}\right)\theta_A \qquad (3.8.5)$$

Note that θ_B has been condensed out of Eq. (3.7.13) in Eq. (3.8.5). Thus, by using Eq. (3.8.5), the degrees of freedom used for the analysis can be reduced if the member is hinged at one end.

If the member is hinged at the A rather than the B end, as shown in

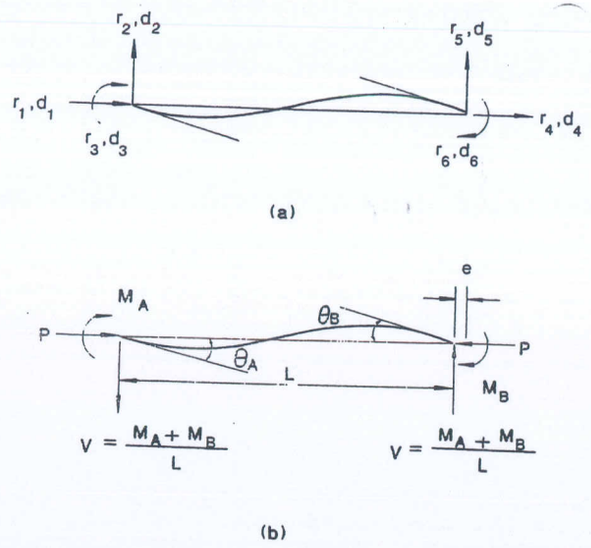

FIGURE 4.9 Element end forces and displacements notations

element end forces and end displacements of a frame member. The end forces and end displacements used in the slope-deflection equation are shown in Fig. 4.9b. By comparing the two figures, we can easily express the following equilibrium and kinematic relationships.

Equilibrium

$$r_1 = P \tag{4.4.1}$$

$$r_2 = -V = -\frac{M_A + M_B}{L} \tag{4.4.2}$$

$$r_3 = M_A \tag{4.4.3}$$

$$r_4 = -P \tag{4.4.4}$$

$$r_5 = \frac{M_A + M_B}{L} \tag{4.4.5}$$

$$r_6 = M_B \tag{4.4.6}$$

Kinematic

$$e = -(d_4 - d_1) \tag{4.4.7}$$

$$\theta_A = d_3 + \left(\frac{d_5 - d_2}{L}\right) \tag{4.4.8}$$

$$\theta_B = d_6 + \left(\frac{d_5 - d_2}{L}\right) \tag{4.4.9}$$

Equations (4.4.1) to (4.4.6) can be written in matrix form as

$$\begin{pmatrix} r_1 \\ r_2 \\ r_3 \\ r_4 \\ r_5 \\ r_6 \end{pmatrix} = \begin{bmatrix} 1 & 0 & 0 \\ 0 & -\frac{1}{L} & -\frac{1}{L} \\ 0 & 1 & 0 \\ -1 & 0 & 0 \\ 0 & \frac{1}{L} & \frac{1}{L} \\ 0 & 0 & 1 \end{bmatrix} \begin{pmatrix} P \\ M_A \\ M_B \end{pmatrix} \tag{4.4.10}$$

Similarly, Eqs. (4.7) to (4.4.9) can be written in matrix form as

$$\begin{pmatrix} e \\ \theta_A \\ \theta_B \end{pmatrix} = \begin{bmatrix} 1 & 0 & 0 & -1 & 0 & 0 \\ 0 & -\frac{1}{L} & 1 & 0 & \frac{1}{L} & 0 \\ 0 & -\frac{1}{L} & 0 & 0 & \frac{1}{L} & 1 \end{bmatrix} \begin{pmatrix} d_1 \\ d_2 \\ d_3 \\ d_4 \\ d_5 \\ d_6 \end{pmatrix} \tag{4.4.11}$$

Equation (4.4.10) and Eq. (4.4.11) can be related by recognizing that

$$P = \frac{EA}{L} e \tag{4.4.12}$$

$$M_A = \frac{EI}{L}(s_{ii}\theta_A + s_{ij}\theta_B) \tag{4.4.13}$$

$$M_B = \frac{EI}{L}(s_{ij}\theta_A + s_{ii}\theta_B) \tag{4.4.14}$$

Equation (4.4.12) relates the axial force P to the axial displacement e of the member, Eqs. (4.4.13) and (4.4.14) are the slope-deflection equations of the member, and s_{ii}, s_{ij} are the stability functions. In writing Eq. (4.4.12), it is tacitly assumed that the effect of member shortening due to the bending curvature is negligible. This assumption is satisfactory for most practical purposes.

Putting Eqs. (4.4.12) to (4.4.14) in matrix form, we have

$$\begin{pmatrix} P \\ M_A \\ M_B \end{pmatrix} = \frac{EI}{L} \begin{bmatrix} \frac{A}{I} & 0 & 0 \\ 0 & s_{ii} & s_{ij} \\ 0 & s_{ij} & s_{ii} \end{bmatrix} \begin{pmatrix} e \\ \theta_A \\ \theta_B \end{pmatrix} \tag{4.4.15}$$

Substituting Eq. (4.4.15) into Eq. (4.4.10), and then substituting Eq. (4.4.11) into the resulting equation, we can relate the element end forces (r_1 to r_6) with the element end displacements (d_1 to d_6) as

$$\begin{pmatrix} r_1 \\ r_2 \\ r_3 \\ r_4 \\ r_5 \\ r_6 \end{pmatrix}_{ns} = \frac{EI}{L} \begin{bmatrix} \frac{A}{I} & 0 & 0 & -\frac{A}{I} & 0 & 0 \\ & \frac{2(s_{ii}+s_{ij})}{L^2} & -\frac{(s_{ii}+s_{ij})}{L} & 0 & \frac{-2(s_{ii}+s_{ij})}{L^2} & \frac{-(s_{ii}+s_{ij})}{L} \\ & & s_{ii} & 0 & \frac{s_{ii}+s_{ij}}{L} & s_{ij} \\ & \text{sym.} & & \frac{A}{I} & 0 & 0 \\ & & & & \frac{2(s_{ii}+s_{ij})}{L^2} & \frac{(s_{ii}+s_{ij})}{L} \\ & & & & & s_{ii} \end{bmatrix}_{ns} \begin{pmatrix} d_1 \\ d_2 \\ d_3 \\ d_4 \\ d_5 \\ d_6 \end{pmatrix} \tag{4.4.16}$$

Symbolically, Eq. (4.4.16) can be written as

$$\mathbf{r}_{ns} = \mathbf{k}_{ns}\mathbf{d} \tag{4.4.17}$$

where the subscript ns is used here to indicate that there is no sidesway in the member. If the member is permitted to sway as shown in Fig. 4.10, an additional shear force equal to $P\,\Delta/L$ will be induced in the member due to the swaying of the member by an amount Δ given by

$$\Delta = d_2 - d_5 \tag{4.4.18}$$

We can relate this additional shear force due to member sway to the member end displacement as

$$\begin{pmatrix} r_1 \\ r_2 \\ r_3 \\ r_4 \\ r_5 \\ r_6 \end{pmatrix}_s = \begin{bmatrix} 0 & 0 & 0 & 0 & 0 & 0 \\ & -\frac{P}{L} & 0 & 0 & \frac{P}{L} & 0 \\ & & 0 & 0 & 0 & 0 \\ & & & 0 & 0 & 0 \\ & \text{sym.} & & & -\frac{P}{L} & 0 \\ & & & & & 0 \end{bmatrix}_s \begin{pmatrix} d_1 \\ d_2 \\ d_3 \\ d_4 \\ d_5 \\ d_6 \end{pmatrix} \tag{4.4.19}$$

or symbolically

$$\mathbf{r}_s = \mathbf{k}_s\mathbf{d} \tag{4.4.20}$$

where the subscript s is used to indicate the quantities due to sidesway of the member.

By combining Eq. (4.4.17) and Eq. (4.4.20), we obtain the general beam-column element force-displacement relationship as

$$\mathbf{r} = \mathbf{k}\mathbf{d} \tag{4.4.21}$$

where

$$\mathbf{r} = \mathbf{r}_{ns} + \mathbf{r}_s \tag{4.4.22a}$$

$$\mathbf{k} = \mathbf{k}_{ns} + \mathbf{k}_s \tag{4.4.22b}$$

$$\mathbf{k} = \frac{EI}{L} \begin{bmatrix} \frac{A}{I} & 0 & 0 & -\frac{A}{I} & 0 & 0 \\ & \frac{2(s_{ii}+s_{ij})-(kL)^2}{L^2} & -\frac{(s_{ii}+s_{ij})}{L} & 0 & \frac{-2(s_{ii}+s_{ij})+(kL)^2}{L^2} & \frac{-(s_{ii}+s_{ij})}{L} \\ & & s_{ii} & 0 & \frac{s_{ii}+s_{ij}}{L} & s_{ij} \\ & \text{sym.} & & \frac{A}{I} & 0 & 0 \\ & & & & \frac{2(s_{ii}+s_{ij})-(kL)^2}{L^2} & \frac{(s_{ii}+s_{ij})}{L} \\ & & & & & s_{ii} \end{bmatrix} \tag{4.4.23}$$

Substituting the expressions for the stability functions (s_{ii}, s_{ij}) in Eq. (4.4.23) and simplifying, we obtain

$$\mathbf{k} = \frac{EI}{L} \begin{bmatrix} \frac{A}{I} & 0 & 0 & -\frac{A}{I} & 0 & 0 \\ & \frac{12}{L^2}\phi_1 & \frac{-6}{L}\phi_2 & 0 & \frac{-12}{L^2}\phi_1 & \frac{-6}{L}\phi_2 \\ & & 4\phi_3 & 0 & \frac{6}{L}\phi_2 & 2\phi_4 \\ & & & \frac{A}{I} & 0 & 0 \\ & \text{sym.} & & & \frac{12}{L^2}\phi_1 & \frac{6}{L}\phi_2 \\ & & & & & 4\phi_3 \end{bmatrix} \tag{4.4.24}$$

The expressions for ϕ_1, ϕ_2, ϕ_3, and ϕ_4 are given in Table 4.1. Note that as P approaches zero, the functions ϕ_1, ϕ_2, ϕ_3, and ϕ_4 become

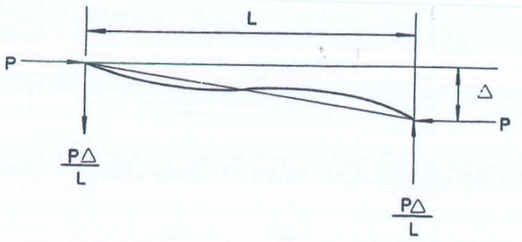

FIGURE 4.10 Additional shear due to swaying of the member

indefinite. However, by using the L'Hospital's rule, it can be shown that these functions will approach unity and Eq. (4.4.24) reduces to the first-order (linear) element stiffness matrix for a frame member.

Also shown in Table 4.1 are the ϕ_i functions expressed in the form of a power series by using the following series expansion for the trigonometric functions:

For compression

$$\sin kL = kL - \frac{(kL)^3}{6} + \frac{(kL)^5}{120} + \cdots \tag{4.4.25a}$$

$$\cos kL = 1 - \frac{kL}{2} + \frac{(kL)^4}{24} + \cdots \tag{4.4.25b}$$

For tension

$$\sinh kL = kL + \frac{(kL)^3}{6} + \frac{(kL)^5}{120} + \cdots \tag{4.4.26a}$$

$$\cosh kL = 1 + \frac{kL}{2} + \frac{(kL)^4}{24} + \cdots \tag{4.4.26b}$$

It has been shown[4] that these power series expressions are convenient and efficient to use in a computer-aided analysis because no numerical difficulties will arise even if the axial force P is small. In addition, the expressions in the series are the same regardless of whether P is tensile or compressive. For most cases, the series will converge to a high degree of accuracy if $n = 10$ is used.

If the axial force in the member is small, Eq. (4.4.24) can be simplified by using a Taylor series expansion for the ϕ_i's. If we retain only the first two terms in the Taylor series, it can be shown that the resulting stiffness

Table 4.1 Expre ns for ϕ_1, ϕ_2, ϕ_3, and ϕ_4

ϕ	P		
	Compressive	Zero	Tensile
ϕ_1	$\frac{(kL)^3 \sin kL}{12\phi_c}$	1	$\frac{(kL)^3 \sinh kL}{12\phi_t}$
ϕ_2	$\frac{(kL)^2(1-\cos kL)}{6\phi_c}$	1	$\frac{(kL)^2(\cosh kL - 1)}{6\phi_t}$
ϕ_3	$\frac{(kL)(\sin kL - kL\cos kL)}{4\phi_c}$	1	$\frac{(kL)(kL\cosh kL - \sinh kL)}{4\phi_t}$
ϕ_4	$\frac{(kL)(kL - \sin kL)}{2\phi_c}$	1	$\frac{(kL)(\sinh kL - kL)}{2\phi_t}$

where

$\phi_c = 2 - 2\cos kL - kL \sin kL$ $\qquad$ $\phi_t = 2 - 2\cosh kL + kL \sinh kL$

Alternatively, the ϕ_i functions can be expressed in the form of power series, as in reference 4:

$$\phi_1 = \frac{1 + \sum_{n=1}^{\infty} \frac{1}{(2n+1)!}[\mp(kL)^2]^n}{12\phi}$$

$$\phi_2 = \frac{\frac{1}{2} + \sum_{n=1}^{\infty} \frac{1}{(2n+2)!}[\mp(kL)^2]^n}{6\phi}$$

$$\phi_3 = \frac{\frac{1}{3} + \sum_{n=1}^{\infty} \frac{2(n+1)}{(2n+3)!}[\mp(kL)^2]^n}{4\phi}$$

$$\phi_4 = \frac{\frac{1}{6} + \sum_{n=1}^{\infty} \frac{1}{(2n+3)!}[\mp(kL)^2]^n}{2\phi}$$

where

$$\phi = \tfrac{1}{12} + \sum_{n=1}^{\infty} \frac{2(n+1)}{(2n+4)!}[\mp(kL)^2]^n$$

Use the minus sign if the axial force is compressive.
Use the plus sign if the axial force is tensile.

matrix th.. .s valid for small axial force is given by

$$\mathbf{k} = \frac{EI}{L}\begin{bmatrix} \frac{A}{I} & 0 & 0 & -\frac{A}{I} & 0 & 0 \\ & \frac{12}{L^2} & \frac{-6}{L} & 0 & \frac{-12}{L^2} & \frac{-6}{L} \\ & & 4 & 0 & \frac{6}{L} & 2 \\ & & & \frac{A}{I} & 0 & 0 \\ & & & & \frac{12}{L^2} & \frac{6}{L} \\ & & & & & 4 \end{bmatrix} \mp \frac{P}{L}\begin{bmatrix} 0 & 0 & 0 & 0 & 0 & 0 \\ & \frac{6}{5} & \frac{-L}{10} & 0 & \frac{-6}{5} & \frac{-L}{10} \\ & & \frac{2L^2}{15} & 0 & \frac{L}{10} & \frac{-L^2}{30} \\ & & & 0 & 0 & 0 \\ & & & & \frac{6}{5} & \frac{L}{10} \\ & & & & & \frac{2L^2}{15} \end{bmatrix} \tag{4.4.27}$$

in which the negative sign preceding the second matrix corresponds to a compressive axial force and the positive sign corresponds to a tensile axial force.

Symbolically, Eq. (4.4.27) can be written as

$$\mathbf{k} = \mathbf{k}_0 + \mathbf{k}_G \tag{4.4.28}$$

where $\mathbf{k}_0$ is the first-order (linear) elastic stiffness matrix and $\mathbf{k}_G$ is the geometric stiffness matrix (sometimes referred to as the initial stress stiffness matrix), which accounts for the effect of the axial force P on the bending stiffness of the member.

The following example will be used to demonstrate the procedure of using the stiffness matrix method to obtain the critical load of frames.

4.4.2 Sway Buckling of a Pinned-Base Portal Frame

The matrix stiffness method is applied here to determine the critical load P_{cr} for the frame shown in Fig. 4.5a. Because of symmetry, we consider only one half of the structure in the analysis. This is shown in Fig. 4.11a together with the structural nodal forces and displacements. To reduce the number of degrees of freedom of the structure, we assume that all members are inextensible (i.e., the change in length due to axial force is neglected). As a result, only four degrees of freedom, are labeled: three rotational degrees of freedom, D_1, D_2, and D_3, and one translational degree of freedom, D_4. The corresponding structural nodal forces, $R_1, \ldots, R_4$, are also shown in Fig. 4.11a. The directions of these

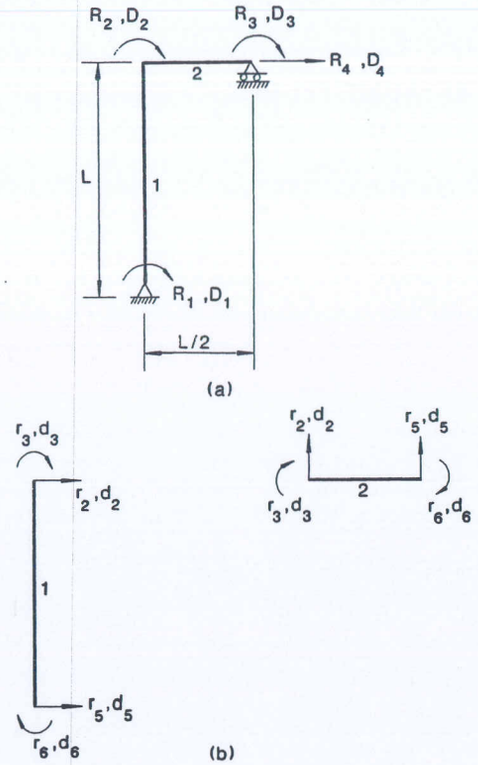

FIGURE 4.11 Structure and member forces and displacements notations

rotations, translations, and forces are shown in their positive sense in the figure.

Because of the assumption of inextensional behavior, the axial force-axial displacement relationship expressed in Eq. (4.4.12) is not valid anymore. As a consequence, the 6×6 element stiffness matrix relating the element end forces to the element end displacements will be reduced to a 4×4 matrix as

$$\mathbf{k} = \frac{EI}{L}\begin{bmatrix} \frac{12}{L^2} & -\frac{6}{L} & -\frac{12}{L^2} & -\frac{6}{L} \\ & 4 & \frac{6}{L} & 2 \\ \text{sym.} & & \frac{12}{L^2} & \frac{6}{L} \\ & & & 4 \end{bmatrix} \mp \frac{P}{L}\begin{bmatrix} \frac{6}{5} & -\frac{L}{10} & -\frac{6}{5} & -\frac{L}{10} \\ & \frac{2L^2}{15} & \frac{L}{10} & -\frac{L^2}{30} \\ \text{sym.} & & \frac{6}{5} & \frac{L}{10} \\ & & & \frac{2L^2}{15} \end{bmatrix} \tag{4.4.29}$$

slope-deflection equation approaches. However, it should be noted that the steps shown above can easily be programmed in a digital computer, and so P_{cr} can be obtained quite conveniently for any type of frame.

4.5 SECOND-ORDER ELASTIC ANALYSIS

In the preceding sections, we determined the load that corresponds to a state of bifurcation of equilibrium of a perfect frame by an eigenvalue analysis. In an eigenvalue analysis, the system is assumed to be perfect. There will be no lateral deflections in the members until the load reaches the critical load P_{cr}. At the critical load P_{cr}, the original configuration of the frame ceases to be stable and with a slight disturbance, the lateral deflections of the members begin to increase without bound as indicated by curve 1 in Fig. 4.2. However, if the system is not perfect, lateral deflections will occur as soon as the load is applied, as shown by curve 2 in Fig. 4.2. For an elastic frame, curve 2 will approach curve 1 asymptotically. To trace this curve, a complete load-deflection analysis of the frame is necessary. A second-order elastic analysis will generate just such load-deflection response of the frame.

In a second-order analysis, such secondary effects as the $P-\delta$ and $P-\Delta$ effects, which we discussed previously in Chapter 3, can be incorporated directly into the analysis procedure. As a result, the use of $P-\delta$ and $P-\Delta$ moment magnification factors (denoted as B_1 and B_2 in Chapter 3) are not necessary.

Because for a second-order analysis the equilibrium equations are formulated with respect to the deformed geometry of the structure, which is not known in advance and is constantly changing with the applied loads, it is necessary to employ an iterative technique to obtain solutions. In a numerical implementation, one of the most popular solution techniques is the incremental load approach. In this approach, the applied load is divided into increments and applied incrementally to the structure. The deformed configurations of the structure at the end of each cycle of calculation is used as the basis for the formulation of equilibrium equations for the next cycle. At a particular cycle of calculation, the structure is assumed to behave linearly. In effect, the nonlinear response of the structure as a result of geometric changes is approximated by a series of linear analyses, the geometry of the structure used in the analysis for a specific cycle is the deformed geometry of the structure corresponding to the previous cycle of calculation. Because of the linearization process, equilibrium may be violated and the external force may not always balance the internal force. This unbalanced force must be reapplied to the structure and the process repeated until equilibrium is satisfied.

For a second-order elastic frame analysis, the iteration process is

summarized in following steps (in the following discussion, a subscript refers to the load step and a superscript refers to the cycle of calculation within each load step):

1. First, discretize the frame into a number of beam-column elements.
2. Next, formulate the element stiffness matrix $\mathbf{k}$ for each and every element. The element stiffness matrix is given in Eq. (4.4.24), or in its approximate form, Eq. (4.4.27). (P can be set equal to zero in these equations for the first cycle of calculations.)
3. Assemble all these element stiffness matrices to form the structure stiffness matrix $\mathbf{K}$.
4. Solve for the incremental displacement vector using

$$\Delta\mathbf{R}_i = \mathbf{K}_i^1 \Delta\mathbf{D}_i^1 \tag{4.5.1}$$

from which

$$\Delta\mathbf{D}_i^1 = (\mathbf{K}_i^1)^{-1} \Delta\mathbf{R}_i \tag{4.5.2}$$

where

$\Delta\mathbf{R}_i$ = prescribed incremental load vector of the i load step
$\mathbf{K}_i^1$ = structure secant stiffness matrix at the beginning of i load step
$\Delta\mathbf{D}_i^1$ = incremental structure nodal displacement vector at i load step.

5. Update the structure nodal displacement vector from

$$\mathbf{D}_i^1 = \mathbf{D}_i + \Delta\mathbf{D}_i^1 \tag{4.5.3}$$

where

$\mathbf{D}_i^1$ = structure nodal displacement vector at the end of the first cycle of calculation at the i load step
$\mathbf{D}_i$ = structure nodal displacement vector at the beginning of the i load step
$\Delta\mathbf{D}_i^1$ = incremental structure nodal displacement vector evaluated at Step 4.

6. Extract the element end displacement vector $\mathbf{d}_i$ from $\mathbf{D}_i^1$ for each and every element in the structure.
7. For each element, evaluate the element axial displacement e and element end rotations θ_A, θ_B from Eqs. (4.4.7) to (4.4.9).
8. For each element, evaluate element axial force P and element end moments M_A, M_B from Eqs. (4.14.12) to (4.4.14).
9. For each element, evaluate element end forces from Eq. (4.4.10).
10. Form the structure internal force vector $\mathbf{R}_i^1$ at the end of the first cycle of calculation by assembling the element end forces evaluated in Step 9 for all the elements.

11. Calculate the external force vector from

$$\mathbf{R}_{i+1} = \mathbf{R}_i + \Delta\mathbf{R}_i \tag{4.5.4}$$

12. Evaluate the unbalanced force $\Delta\mathbf{Q}_i^1$ at the end of the cycle from

$$\Delta\mathbf{Q}_i^1 = \mathbf{R}_{i+1} - \mathbf{R}_i^1 \tag{4.5.5}$$

13. Using the current value of axial force P, update the element stiffness matrix $\mathbf{k}$ for each and every element. Assemble $\mathbf{k}$ for all the elements to form an updated secant structure stiffness matrix $\mathbf{K}_i^2$. Evaluate the incremental displacement vector $\Delta\mathbf{D}_i^2$ from

$$\Delta\mathbf{D}_i^2 = (\mathbf{K}_i^2)^{-1}\,\Delta\mathbf{Q}_i^1 \tag{4.5.6}$$

where $\Delta\mathbf{Q}_i^1$ is the unbalanced force vector calculated in the previous cycle of calculation.

14. Update the structure nodal displacement vector from

$$\mathbf{D}_i^2 = \mathbf{D}_i + \sum_{k=1}^{2} \Delta\mathbf{D}_i^k \tag{4.5.7}$$

15. Extract the element end displacement vector $\mathbf{d}_i$ from $\mathbf{D}_i^2$ calculated in Eq. (4.5.7) for each and every element. Update e, θ_A, and θ_B and, hence, P, M_A, and M_B as done in Steps 7 and 8 for all elements in the frame.
16. Update the element end forces for all the elements and form the new structure internal force vector $\mathbf{R}_i^2$.
17. Evaluate the new unbalanced force $\Delta\mathbf{Q}_i^2$ from

$$\Delta\mathbf{Q}_i^2 = \mathbf{R}_{i+1} - \mathbf{R}_i^2 \tag{4.5.8}$$

18. Repeat Steps 13 through 17 as many times as possible until convergence. Convergence is said to have been attained if the unbalanced force $\Delta\mathbf{Q}_1^j$, where the superscript j refers to the j cycle of calculation, falls within a prescribed tolerance.
19. After convergence the structure nodal displacement at the end of the i load step is obtained by

$$\mathbf{D}_{i+1} = \mathbf{D}_i^n = \mathbf{D}_i + \sum_{k=1}^{n} \Delta\mathbf{D}_i^k \tag{4.5.9}$$

20. Prescribe another load increment and repeat Step 2 to 19.

A schematic representation of the above procedure is shown in Fig. 4.12a,b for a one degree of freedom structure. In performing the above procedure, the complete load-deflection response of the frame can be traced, and the stability limit point is obtained as the peak point of this load-deflection curve.

As the stability limit point is approached in the analysis, convergence

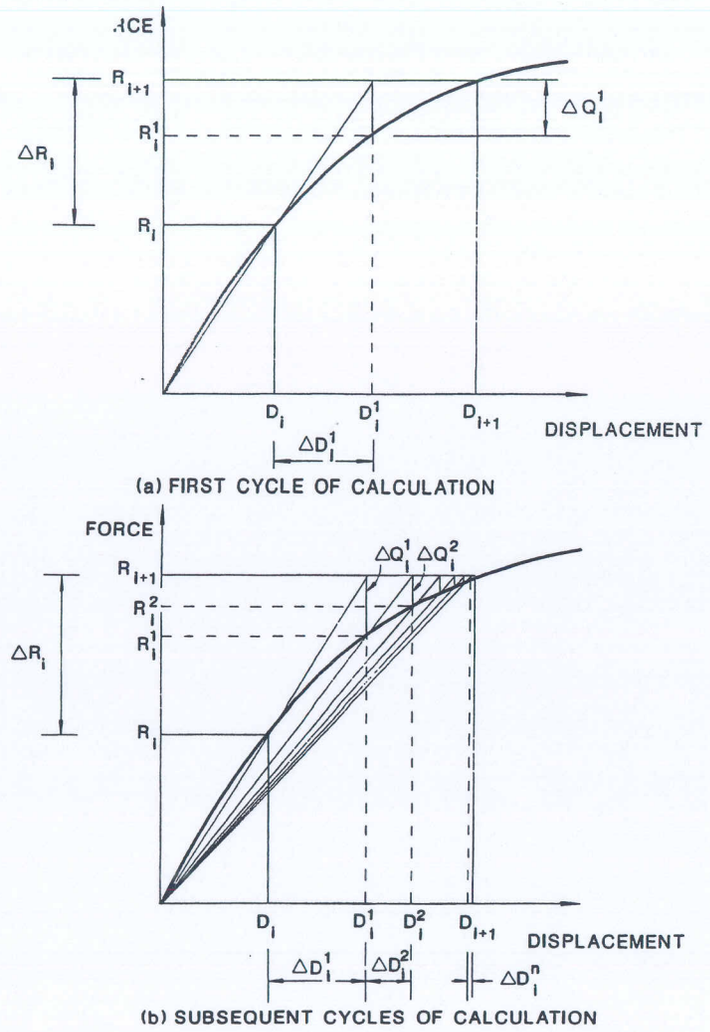

FIGURE 4.12 Iteration technique for second-order elastic frame analysis

of the solution may be slow. To facilitate convergence, a smaller load increment should be used.

The numerical procedure described above can be programmed in a computer. By using the computer to perform a second-order analysis, the design moments for the members can be obtained directly. Comparative studies using second-order elastic analysis and first-order elastic analysis in conjunction with B_1, B_2 moment amplification factors described on Chapter 3 have been made.[4,8] It was demonstrated that for rigidly

Strategies for Tracing the Nonlinear Response Near Limit Points

E. RAMM
Universität Stuttgart, Germany

Abstract

For the prebuckling range an extensive literature of effective solution techniques exists for the numerical solution of structural problems but only a few algorithms have been proposed to trace nonlinear response from the pre-limit into the post-limit range. Among these are the simple method of suppressing equilibrium iterations, the introduction of artificial springs, the displacement control method and the "constant-arc-length method" of Riks/Wempner. It is the purpose of this paper to review these methods and to discuss the modifications to a program that are necessary for their implementation. Selected numerical examples show that a modified Riks/Wempner method can be especially recommended.

1. Introduction

Usually postcritical states are not tolerated in the design of a structure. However, the prediction of response in this range may still be of great value. A typical example is the imperfection sensitivity of certain structures which in general is directly related to the postcritical response. In particular this is true for structures exhibiting a decreasing post-limit characteristic. This may result in a dynamic snap-through or snap-back phenomenon depending on whether the load or the displacement controls the system. However, a static analysis traces the whole postcritical range allowing for a better judgement of the overall structural response.

It is well known that the usually applied Newton-Raphson iteration methods are not very efficient and often fail in the neighborhood

of critical points. The stiffness matrix approaches singularity resulting in an increasing number of iterations and smaller and smaller load steps. Finally the solution diverges. In recent years several strategies have been proposed to overcome these problems and to trace the response beyond the critical point.

It is the purpose of this paper to describe some of the most commonly used techniques. These are the method of suppressing the equilibrium iterations in the neighborhood of the critical point, the method of artificial springs, the displacement control technique and the "constant - arc - length method" of Riks [1], [2] and Wempner [3]. In particular an attempt is made to show the correlation of the latter procedures. Special emphasis is given to some modifications of the Riks/Wempner method leading to an efficient iterative technique throughout the entire range of loading and not only near the critical point. Other methods for solving the same type of problem, e. g. the perturbation method or dynamic relaxation, are not studied.

The discussion refers to limit points only. Bifurcation problems may be included either by introducing a small perturbation in geometry or load (imperfect approach) or by superimposing on the displacement field of the critical load a part of the eigenmode (perfect approach). The procedures are described in conjunction with the Newton-Raphson method in its standard or modified versions. A combination with accelerated quasi Newton methods is possible. Proportional loading is assumed but few changes are necessary for non proportional loading.

2. Starting Point and Notation

The study is based on the incremental/iterative solution procedure in a nonlinear finite element analysis; i. e. the nonlinear problem is stepwise linearized and the linearization error is corrected by additional equilibrium iterations, see for instance [4]. A left superscript indicates the current configuration of the total displacements ${}^{m}\mathbf{u}$, the

load vector ${}^{m}\mathbf{P}$, the internal forces ${}^{m}\mathbf{F}$ and the out-of-balance forces ${}^{m}\mathbf{R}$. For proportional loading the loads may be expressed by one load factor ${}^{m}\lambda$

$$ {}^{m}\mathbf{P} = {}^{m}\lambda \cdot \mathbf{P} \qquad (1) $$

where $\mathbf{P}$ is a vector of reference loads. Within one increment from configuration m to m + 1, the positions i and j = i + 1, before and after an arbitrary iteration cycle, are distinguished (figure 1).

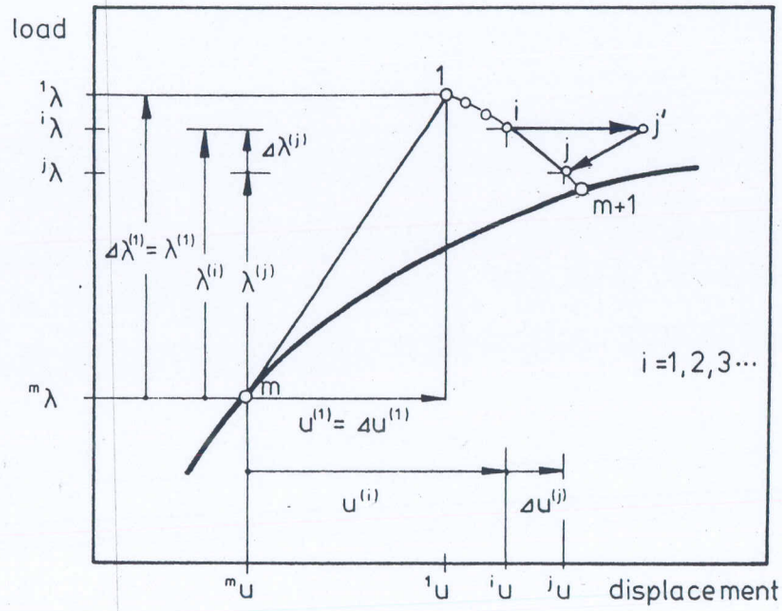

Figure 1: Notation

The total increments between positions m and i are denoted by $\mathbf{u}^{(i)}$, $\mathbf{P}^{(i)}$ and $\lambda^{(i)}$ whereas the changes in increments from i to j are denoted by $\Delta\mathbf{u}^{(j)}$, $\Delta\mathbf{P}^{(j)}$ and $\Delta\lambda^{(j)}$, respectively:

$$ {}^{j}\mathbf{P} = {}^{m}\mathbf{P} + \underbrace{\mathbf{P}^{(i)} + \Delta\mathbf{P}^{(j)}}_{\mathbf{P}^{(j)}} \quad \text{and} \quad {}^{j}\lambda = {}^{m}\lambda + \underbrace{\lambda^{(i)} + \Delta\lambda^{(j)}}_{\lambda^{(j)}} $$

$$ {}^{j}\mathbf{u} = {}^{m}\mathbf{u} + \underbrace{\mathbf{u}^{(i)} + \Delta\mathbf{u}^{(j)}}_{\mathbf{u}^{(j)}} \qquad (2) $$

In view of the fact that iteration takes place in the displacement and load space the load level may change from one iterate to the other. In this case an intermediate position j' for the same load level ${}^{j'}\lambda = {}^{i}\lambda$ is introduced before the final state j is reached (figure 1).

Supposedly configuration i has already been determined and the incremental equilibrium equations may be expressed by the linearized stiffness expression.

$$ {}^{i}K \cdot \Delta u^{(j)} = \Delta P^{(j)} + {}^{i}P - {}^{i}F \qquad (3\,a) $$

If the out-of-balance forces ${}^{i}R = {}^{i}P - {}^{i}F$ are inserted

$$ {}^{i}K \cdot \Delta u^{(j)} = \Delta\lambda^{(j)} \cdot P + {}^{i}R \qquad (3\,b) $$

The tangent stiffness matrix ${}^{i}K$ at position i may include all possible nonlinear effects. It may be kept unchanged through several iteration cycles following the modified Newton-Raphson technique. Eq. (3) is the basic relation used as the starting point for the different iterative techniques described below.

The static stability criterion indicates a limit or bifurcation point by

$$ {}^{c}K \cdot \Delta u^{c} = 0 \qquad (4) $$

where Δu^{c} is the eigenmode of the critical point. The singularity is usually checked by the determinant

$$ \det {}^{c}K = 0 \qquad (5) $$

The determinant can easily be calculated as the product of all diagonal terms in the triangularized matrix during Gaussian elimination. Note that a positive determinant is not a sufficient criterion for stable equilibrium. Rather, the signs of the diagonal terms should be monitored to detect negative eigenvalues. This is the point when the limit load is passed and unloading should start.

3. Description of Some Iterative Techniques

3.1 Suppressing Equilibrium Iterations

As mentioned the equilibrium iterations usually break down near the limit point even if the load increment is small. The simplest way of avoiding this difficulty is to suppress the iterations in the critical zone. This procedure is used with great success by Bergan [5] who introduced the "current stiffness parameter" to guide the algorithm (figure 2).

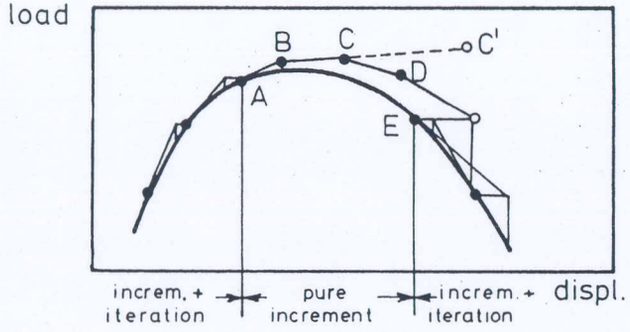

Figure 2: Suppressing iterations due to Bergan [5]

At a prescribed value of the stiffness parameter the iteration procedure is discontinued (point A). Then pure incrementation is used. If the Euclidean norm of the displacement increments exceeds a certain prescribed limit (point C') load and displacements are linearly scaled back (point C). Here negative diagonal elements may be detected in which case negative load increments are applied (point D). The iteration procedure is resumed when the stiffness parameter again reaches its prescribed value (point E). The limit point is located by a zero value of the stiffness parameter. The technique requires very small load increments to avoid drifting away from the equilibrium path.

3.2 Artificial - Spring - Method

This method was developed for frames by Wright and Gaylord [6]

to shell structures by the author [8]. The technique is based on the observation that a snap-through problem may be transformed into one with a positive definite characteristic if linear artificial springs are added to the system (figure 3).

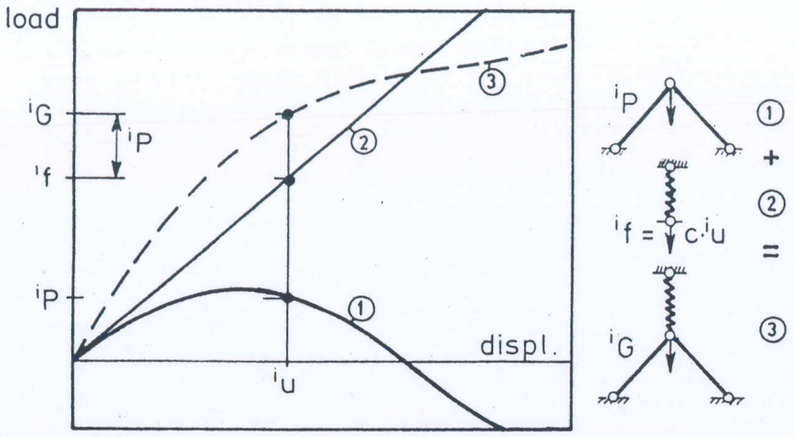

Figure 3: Artificial spring method

The method is described in detail in appendix I. It is an essential requirement that a separation of the real problem must be possible after the analysis of the stiffened system is obtained, i. e. for each stage only one load-reduction factor is defined. Furthermore the symmetry of the augmented stiffness matrix should be preserved. These requirements lead to springs at all loaded degrees of freedom, which are coupled, and depend on one single reference stiffness. This parameter has to be found by trial. The coupling of all artificial stiffnesses may destroy the banded nature of the stiffness matrix. In [8] the elements outside the band were omitted from the stiffness matrix but were retained on the right hand side to find the proper internal forces. Augmenting the spring stiffnesses on the band by a factor of three to five accelerates the convergence.

Because the "nonlinearity" of the system is diminished by the artificial springs the total number of iterations can nevertheless be reduced compared to the analysis without springs. Numerical experience shows that the method is successful only in real snap-through

problems where the springs can keep the destabilizing structure alive. The method cannot be recommended for structures with local buckling or when a tendency to bifurcation is present.

3.3 Displacement - Control

The most often used method to avoid the singularity at the critical point is the interchange of dependent and independent variables. Here a single displacement component selected as a controlling parameter is prescribed and the corresponding load level is taken as unknown. The procedure was introduced first by Argyris [9] but in the meantime has been modified by several authors.

For simplicity let us assume that the stiffness expression, eq. (3), is reordered so that the prescribed component $\Delta u_2^{(j)} = \hat{u}_2$ is the last one in the displacement vector $\Delta \mathbf{u}^{(j)}$. Then equation (3) may be decomposed into two parts

$$^i\begin{bmatrix} K_{11} & K_{12} \\ K_{21} & K_{22} \end{bmatrix} \begin{bmatrix} \Delta u_1 \\ \Delta u_2 \end{bmatrix}^{(j)} = \Delta\lambda^{(j)} \cdot \begin{bmatrix} P_1 \\ P_2 \end{bmatrix} + {}^i\begin{bmatrix} R_1 \\ R_2 \end{bmatrix} \tag{6}$$

Interchanging the variables

$$\begin{bmatrix} ^iK_{11} & -P_1 \\ ^iK_{21} & -P_2 \end{bmatrix} \begin{bmatrix} \Delta u_1 \\ \Delta\lambda \end{bmatrix}^{(j)} = {}^i\begin{bmatrix} R_1 \\ R_2 \end{bmatrix} - {}^i\begin{bmatrix} K_{12} \\ K_{22} \end{bmatrix} \hat{u}_2 \tag{7}$$

it is obvious that the loss of the symmetrical and banded structure of the stiffness matrix is a severe handicap. Later it was recognized that the solution of eq. (7) could be formed in two parts. The first line of eq. (7)

$$^iK_{11} \cdot \Delta u_1^{(j)} = \Delta\lambda^{(j)} \cdot P_1 + {}^iR_1 - {}^iK_{12} \cdot \hat{u}_2 \tag{8}$$

is linear in the unknown increment at the load parameter $\Delta\lambda^{(j)}$.

Therefore its solution may be decomposed into (figure 4)

$$\Delta u_1^{(j)} = \Delta\lambda^{(j)} \cdot \Delta u_1^{(j)\,I} + \Delta u_1^{(j)\,II} \qquad (9)$$

corresponding to the two parts of the right hand side of eq. (8). That is, both solutions are obtained simultaneously using two different "load" vectors

$$^{i}K_{11} \cdot \Delta u_1^{(j)I} = P_1 \qquad (10\,a)$$

$$^{i}K_{11} \cdot \Delta u_1^{(j)II} = {}^{i}R_1 - \underline{{}^{i}K_{12} \cdot \hat{u}_2} \qquad (10\,b)$$

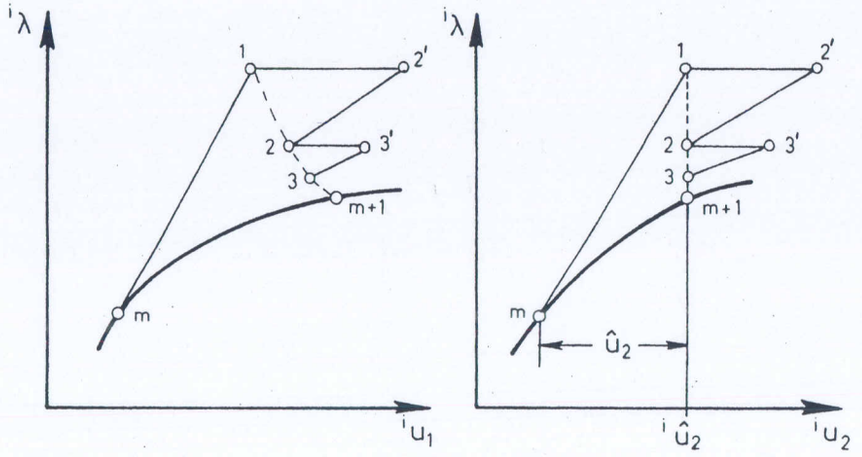

Figure 4: Displacement - Control Method

The displacement increment $\Delta u_1^{(j)}$, eq. (9), is introduced into the second part of eq. (7). This allows the determination of the load parameter $\Delta\lambda^{(j)}$:

$$\Delta\lambda^{(j)} = \frac{-\,{}^{i}R_2 + {}^{i}K_{21} \cdot \Delta u_1^{(j)\,II} + \underline{{}^{i}K_{22} \cdot \hat{u}_2}}{P_2 - {}^{i}K_{21} \cdot \Delta u_1^{(j)\,I}} \qquad (11)$$

Thus instead of solving an unsymmetrical equation the modified stiffness expression, eq. (8), is analysed for two right hand sides provided that $^{i}K_{11}$ is not singular. Since the displacement $\hat{u}_2$ is held fixed during the iteration the underlined terms in equations (10 b) and (11) are omitted in all further iteration cycles.

This modified displacement control method was described first by Pian and Tong [10] without mentioning the out-of-balance terms. Zienkiewicz [11] refers to the standard programming technique and gives a physical interpretation of the two step method. Sabir and Lock [12] explicitly introduced the out-of-balance terms into the formulation. The method was also described in detail by Stricklin et al. [13]. A similar procedure has been applied by Nemat-Nasser and Shatoff [14] who used a direct substitution method instead of the Newton-Raphson technique.

A valuable simplification was utilized by Batoz and Dhatt [15]. Since the technique above described requires a modification of the stiffness matrix ($^{i}K \rightarrow {}^{i}K_{11}$) the authors point out that it is not very likely to obtain exactly the singular point. Hence the original matrix ^{i}K may still be used and equations (10) are replaced by

$$^{i}K \cdot \Delta u^{(j)\,I} = P \qquad (12\,a)$$

$$^{i}K \cdot \Delta u^{(j)\,II} = {}^{i}R \qquad (12\,b)$$

where the underlined term in eq. (10 b) is not required to be formed. Again both solutions are added:

$$\Delta u^{(j)} = \Delta\lambda^{(j)} \cdot \Delta u^{(j)\,I} + \Delta u^{(j)\,II} \qquad (13\,a)$$

The vector includes also the prescribed component

$$\Delta u_2^{(j)} = \Delta\lambda^{(j)} \cdot \Delta u_2^{(j)\,I} + \Delta u_2^{(j)\,II} = \hat{u}_2 \qquad (13\,b)$$

This constraint equation used in the first iteration cycle ($m \rightarrow j = 1$)

allows the determination of the incremental load parameter

$$\Delta\lambda^{(1)} = \frac{\hat{u}_2 - \Delta u_2^{(1)\,II}}{\Delta u_2^{(1)\,I}} \qquad (14)$$

Supposedly the structure is in an equilibrium state at the beginning of a step so the out-of-balance forces vanish and so does $\Delta u_2^{(j)\,II}$. Then $\Delta\lambda^{(1)}$ is simply a scaling factor providing the constraint $\underset{\Delta\lambda^{(1)}}{\Delta} u_2^{(1)} = \hat{u}_2$. Batoz and Dhatt [15] even drop this first cycle. They update the displacement field only by its component $\Delta u_2^{(1)}$ and start to iterate.

For all further cycles $u_2^{(j)}$ does not change i.e. $\Delta u_2^{(j)}$ is zero and $\Delta\lambda^{(j)}$ is

$$\Delta\lambda^{(j)} = -\frac{\Delta u_2^{(j)\,II}}{\Delta u_2^{(j)\,I}} \qquad j = 2,3 \cdots\cdots \qquad (15)$$

Applying the modified Newton-Raphson technique eq. (12 a) needs to be solved only when the stiffness matrix is updated. Then no additional computer time is required and the only additional vector stored is $\Delta\mathbf{u}^{(1)\,I}$. The iteration is continued until all other displacement components are adjusted and the new equilibrium position is found (fig. 4).

The displacement control method is usually used only in the neighborhood of the critical point although it may be applied throughout the entire load range. Obviously the method fails whenever the structure snaps back from one load level to a lower one (see example 5.2). Some knowledge of the failure mode is required for a proper choice of the controlling displacement. It might even be necessary to change the prescribed parameter. Therefore an obvious modification is to relate the procedure to a measure including all displacements rather than to one single component. This is discussed in the next section.

3.4 Modified Constant - Arc - Length - Method of Riks/Wempner

This iterative technique has been independently introduced by Riks [1], [2] and Wempner [3]. Both authors limit the load step $\Delta\lambda^{(1)}$

by the constraint equation

$$\Delta\mathbf{u}^{(1)T}\,\Delta\mathbf{u}^{(1)} + (\Delta\lambda^{(1)})^2 = ds^2 \qquad (16)$$

That is, the generalized "arc length" of the tangent at m is fixed to a prescribed value ds. Then the iteration path follows a "plane" normal to the tangent (figure 5); so the scalar product of the tangent $\vec{t}^{(1)}$ and the vector $\Delta\vec{u}^{(j)}$ containing the unknown load and displacement increments must vanish:

$$\vec{t}^{(1)} \cdot \Delta\vec{u}^{(j)} = 0 \qquad (17a)$$

$\vec{t}^{(1)} = (\Delta u^{(1)}, \Delta\lambda^{(1)})$

or in matrix notation

$$\Delta\mathbf{u}^{(1)T}\,\Delta\mathbf{u}^{(j)} + \Delta\lambda^{(1)}\,\Delta\lambda^{(j)} = 0 \qquad (17b)$$

$j = 2,3 \cdots\cdots$

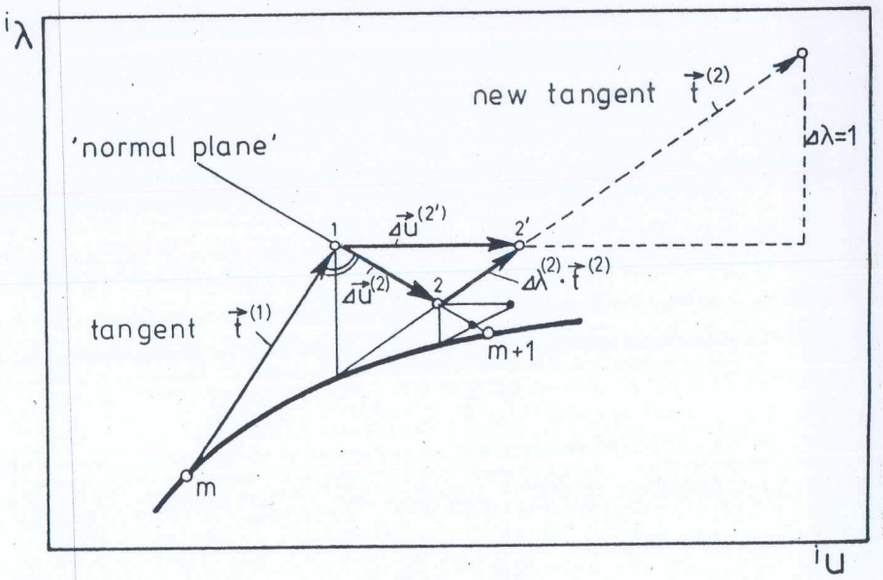

Figure 5: Constant - Arc - Length Method

The constraint equations originally were added to the incremental stiffness expression destroying symmetry and the banded structure of the matrix. It was realized by Wessels [16] based on geometrical considerations that these difficulties could be removed by a two step technique similar to that described in the previous section. It is this idea followed in this study. *)

Again the unknown vector $\Delta \vec{u}^{(j)}$ is formed in two parts

$$\Delta \vec{u}^{(j)} = \Delta\lambda^{(j)} \cdot \vec{t}^{(j)} + \Delta \vec{u}^{(j')} \tag{18 a}$$

or in matrix notation equivalent to eq. (13 a).

$$\Delta \mathbf{u}^{(j)} = \Delta\lambda^{(j)} \cdot \Delta \mathbf{u}^{(j)\,I} + \Delta \mathbf{u}^{(j)\,II} \tag{18 b}$$

Also here $\Delta \mathbf{u}^{(j)\,I}$ and $\Delta \mathbf{u}^{(j)\,II}$ are obtained by equations (12) using either the reference load vector $\mathbf{P}$ ($\Delta\lambda = 1$) or the out-of-balance forces ${}^{i}\mathbf{R}$ as right hand sides. Then eq. (18) is inserted into the constraint eq. (17) and solved for the unknown load increment $\Delta\lambda^{(j)}$

$$\Delta\lambda^{(j)} = - \frac{\Delta \mathbf{u}^{(1)T} \cdot \Delta \mathbf{u}^{(j)\,II}}{\Delta \mathbf{u}^{(1)T} \cdot \Delta \mathbf{u}^{(j)\,I} + \Delta\lambda^{(1)}} \tag{19}$$

Geometrically this is the intersection j of the new tangent $\vec{t}^{(j)}$ with the "normal plane" (figure 5). Eq. (19) is equivalent to eq. (15) but contains the influence of all displacement components in an integral sense. The load increment $\Delta\lambda^{(1)}$ in the denominator, which obviously has another dimension, expresses the different scaling of the load axis with respect to the displacement space. It may be seen for the one degree-of-freedom system in figure 6 a that a low value $\Delta\lambda^{(1)}$ tends to a displacement control and a large value to a load control of the iteration. In many degree-of-freedom systems the value $\Delta\lambda^{(1)}$ in eq. (19) does not play an important role and may be suppressed.

*) During the preparation of this study the author became aware of the valuable paper by Crisfield [17] devoted to the same subject.

Again the modified Newton-Raphson technique simplifies the method because eq. (12 a) is solved only once at the beginning of the step and may even be replaced by the first solution $\Delta \mathbf{u}^{(1)}$:

$$\frac{\Delta\lambda^{(j)}}{\Delta\lambda^{(1)}} = - \frac{\Delta \mathbf{u}^{(1)T} \cdot \Delta \mathbf{u}^{(j)\,II}}{\Delta \mathbf{u}^{(1)T} \cdot \Delta \mathbf{u}^{(1)} + (\Delta\lambda^{(1)})^2} \tag{20}$$

Instead of iterating in the "plane" normal to the tangent $\vec{t}^{(1)}$ it might be useful to define a "sphere" with a center at m and a radius ds [17] (see appendix II). Alternatively the "normal plane" may be updated in every iteration cycle (figure 6 b). That is, in eq. (19) $\Delta \mathbf{u}^{(1)}$ is replaced by the total increment $\mathbf{u}^{(i)}$. It was found that except for very large load steps the differences resulting from these formulations are minor.

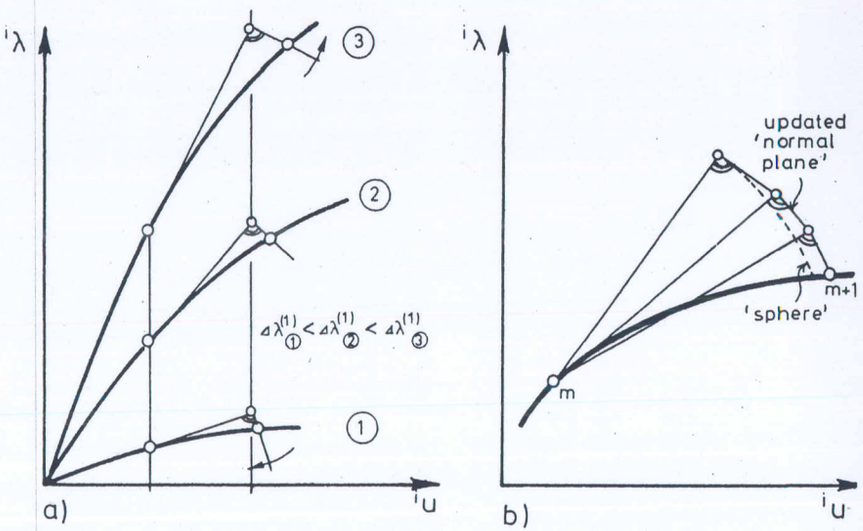

Figure 6: Modification of constant - arc - length method

Numerical experience has shown that this iterative technique is very efficient in the entire load range particularly when automatic load incrementation based on eq. (16) is used. The only additional storage required is the vector $\Delta \mathbf{u}^{(1)}$. The extra computer time is negligible.

In addition to the "constant-arc-length" the step size may be scaled by relating the number of iterations, n_i, used in the previous step to a desired value, $\hat{n}_i$. It was found that a factor $\hat{n}_i/n_i$ results in oscillations in the number of iterations required from step to step so that $\sqrt{\hat{n}_i/n_i}$ is recommended. If material nonlinearities are involved smaller load steps should be defined to avoid drifting. Whenever a negative element in the triangularized matrix is encountered unloading is initiated. The convergence may be either monotonic or alternating and may in some cases be slow. Then relaxation factors may accelerate the iteration process. For instance, in the alternating case a cut-back of the next load change to 50 % resulted in a considerable improvement.

4. Summary of the Displacement Control and Modified Riks/Wempner Method

The algorithms for the displacement control method and the modified Riks/Wempner method differ only in the equation used for the evaluation of $\Delta\lambda^{(j)}$. The algorithm is summarized as follows:

1. Select a basic load increment as the reference load $\mathbf{P}$, thus defining the length ds in the first step (eq. 16).
2. In any step:
   a) Solve the equilibrium equations for $\mathbf{P}$ and linearly scale the load and displacements to produce the length ds. This determines $\Delta\lambda^{(1)}$, $\Delta\mathbf{u}^{(1)}$.
   b) Adjust the step size to the desired number of iterations $\hat{n}_i$, e. g. $\sqrt{\hat{n}_i/n_i}$.
   c) Check the triangularized matrix for unloading.
3. a)* Update the stiffness matrix ${}^{i}\mathbf{K}$
   b) and, simultaneously, determine the out-of-balance forces ${}^{i}\mathbf{R}$.
   c)* Solve for $\mathbf{P}$ to determine $\Delta\mathbf{u}^{(j)\,I}$.
   d) and, simultaneously, solve for the out-of-balance forces ${}^{i}\mathbf{R}$ to determine $\Delta\mathbf{u}^{(j)\,II}$.

Note: * indicates a step which is omitted in the modified Newton

4. Use constraint eq. (15) or (19) to determine the load increment $\Delta\lambda^{(j)}$ and eq. (13 a) ≡ eq. (18 b) to determine displacement increments $\Delta\mathbf{u}^{(j)}$. (If needed use acceleration factors.)
5. Update the load level and the displacement field.
6. Repeat steps 3 - 5 until the desired accuracy is achieved.
7. Reformulate the stiffness matrix and start a new step by returning to 2.

5. Numerical Examples

The examples have been analysed on CDC 6600/Cyber 174 computers using the nonlinear finite element code NISA [18]. The geometrical nonlinearity is based on the total Lagrangian formulation. For the arch example, an 8 node isoparametric plane stress element is used [4]. The plate and shell structures are idealized by degenerated isoparametric elements developed in [8], [19]. The modified Riks/Wempner method, in combination with the modified Newton-Raphson technique, has been applied exclusively. The ratio of the change of the incremental displacements to the total displacement increments, using Euclidean norms, is used for the convergence criterion.

5.1 Shallow Arch

The shallow circular arch under uniform pressure (figure 7) has already been analysed in [8] applying the artificial spring method (c_{11} = 28 lb/in), see also [7]. Ten 8 node isoparametric plane stress elements were used for one half of the arch. The analysis with a basic load of $\bar{p}$ = 0.3 and using the constant-arc-length constraint shows the typical step size reduction in the neighborhood of the limit point. Thirty steps with 1 to 2 iterations per step were needed. The analysis has been repeated for a basic load step of $\bar{p}$ = 1.0. The step size has been adjusted by the factor $\sqrt{\hat{n}_i/n_i}$ with a desired number of iterations $\hat{n}_i$ = 5. In addition, the load increment was reduced to 50 % whenever

sufficient. The number of iterations required are indicated in the figure. The diagram also shows the starting point in each step after the first Newton-Raphson iterate. Compared to the artificial spring technique considerable savings are achieved.

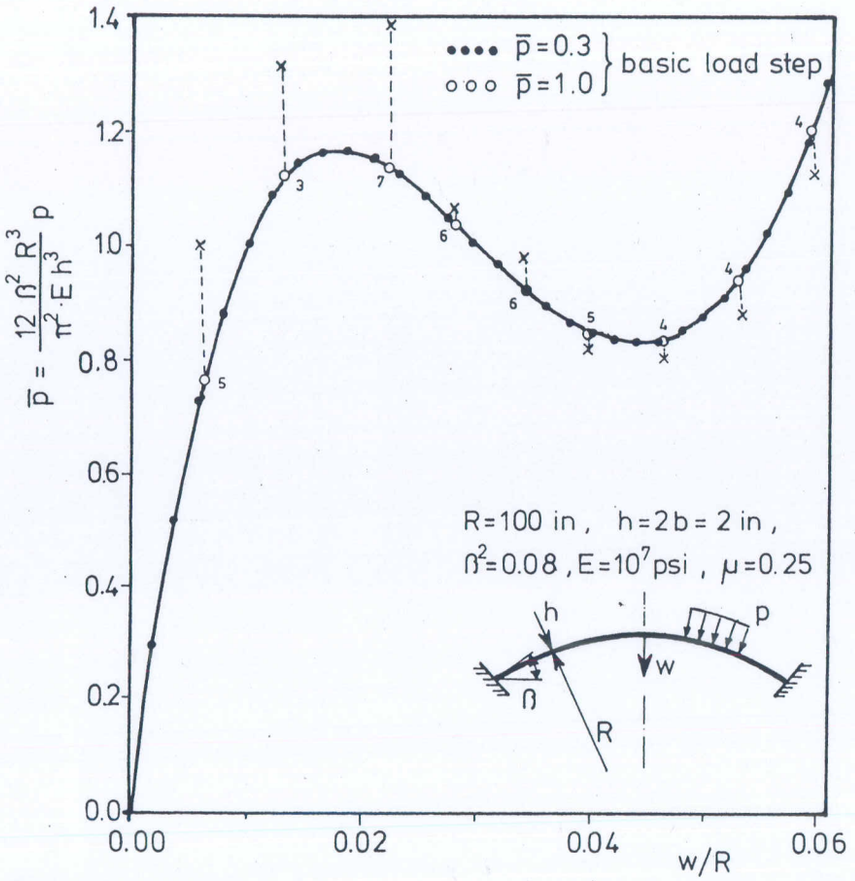

Figure 7: Shallow circular arch

5.2 Shallow Cylindrical Shell

The shallow cylindrical shell under one concentrated load (figure 8) is hinged at the longitudinal edges and free at the curved boundaries. The structure exhibits snap-through as well as snap-back phenomena with horizontal and vertical tangents. The shell has been analysed by

Sabir and Lock [20] who used a combination of the displacement and load control techniques. In the present study one quarter of the shell has been idealized by four 16 node bicubic degenerated shell elements. As the basic load step, P^1 = 0.4 kN was chosen. Again the load steps were adjusted with $\sqrt{n_i/n_1}$ and the acceleration scheme described for the arch was applied. The entire load deflection diagram is obtained in one solution with 15 steps and 3 to 9 iterations per step as indicated in the figure. If the acceleration technique was not used the number of iterations increased considerably especially at the minimum load.

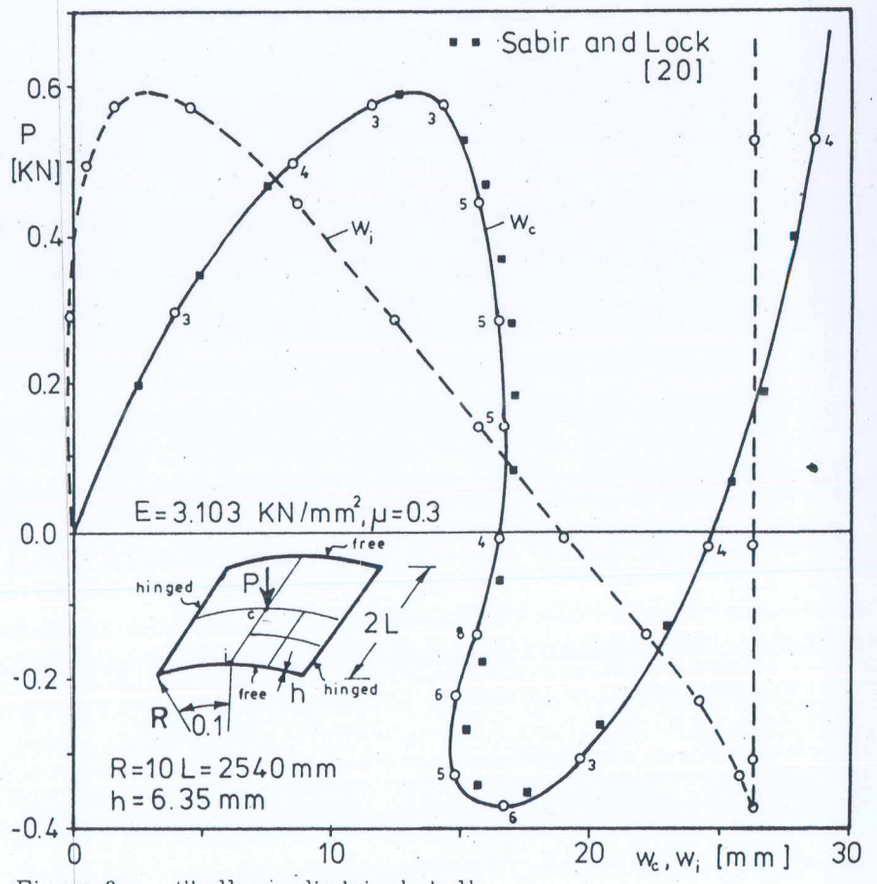

Figure 8: Shallow cylindrical shell

This part of the load-deflection curve is numerically difficult because

the free edge. The structure has also been analysed using 36 bilinear 4 node degenerated elements in combination with an uniform 1 x 1 reduced integration scheme. Approximately the same results have been obtained but at about 20 % of the CP-time.

5.3 Elastic - Plastic Buckling of a Plate

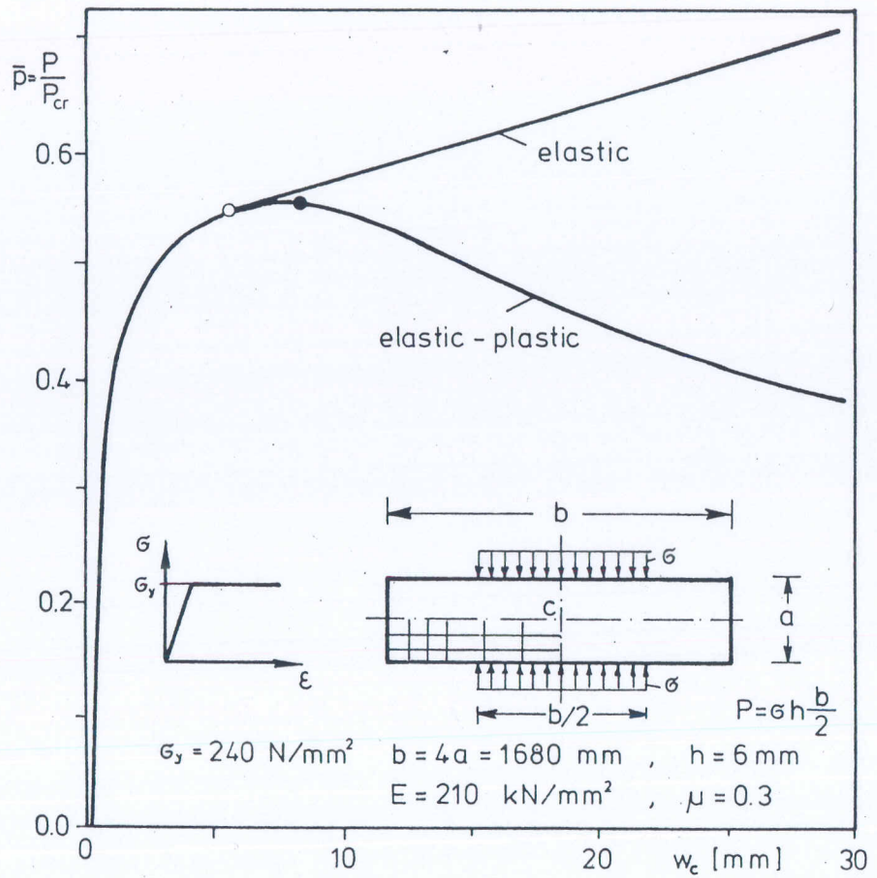

Figure 9: Buckling of a long plate

The simply supported plate shown in figure 9 has an aspect ratio of $\alpha = 1/4$ and is loaded only on its middle part. The plate has an initial geometrical imperfection, defined by a double sin-function, with a maximum amplitude of 0.294 mm. The yield limit σ_y of the elastic-ideally plastic steel is 240 N/mm². Eighteen bicubic degenerated elements unevenly spaced were used for one quarter of the plate. The thickness was divided into seven layers. The total load P is non-dimensionalized with the linear elastic buckling load P_{cr} of the plate with uniform load on the entire boundary:

$$P_{cr} = k \cdot b \cdot \frac{\pi^2 \cdot E \cdot h^3}{12 \cdot (1-\mu^2) \cdot a^2} \quad ; \quad k = (1 + \alpha^2)^2 \qquad (21)$$

The basic load step chosen was $\bar{p} = 0.25$. In figure 9 the normalized load is plotted versus the center lateral displacement. The plate fails under combined geometrical and material failure. The initial yield point at a deflection of about 6 mm is immediately followed by the limit point at about 8.3 mm. Thirty steps with 1 or 2 iterations per step were used. The elasto-plastic analysis was supplemented by a purely elastic solution also shown in the figure. Here the typical increasing postbuckling response of plates is recognized.

5.4 Cylindrical Shell under Wind Load

The buckling analysis of the closed cylindrical shell under wind load (figure 10) studied in [21] has been extended to the postbuckling range.

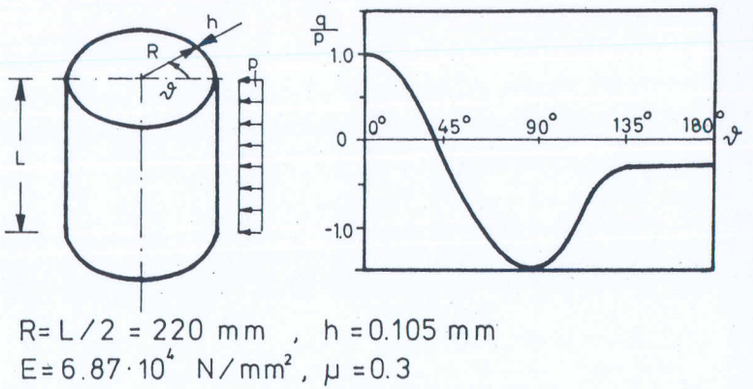

Figure 10: Geometry and load function of a cylindrical shell

The extremely thin structure with a radius to thickness ratio of over 2000 is simply supported at both ends. The variation of the wind load defined in figure 10 is taken as constant over the length of the cylinder. The maximal load p at the stagnation point is normalized to the linear buckling load of the shell under uniform pressure

$$p_{cl} = \frac{0.918 \cdot E(\frac{h}{R})^2}{\frac{L}{R}\sqrt{\frac{R}{h}} - 0.657} \qquad \bar{p} = \frac{p}{p_{cl}} \qquad (22)$$

One quarter of the shell is idealized by 2 x 18 bicubic 16 node elements. Two elements of unequal length are used in the axial direction, while the 18 elements in the circumferential direction are concentrated near the stagnation zone. The first load increment defined the basic step size as $\bar{p} = 0.25$. Both the perfect and an imperfect shell have been analysed. Figure 11 shows the displacement pattern of one quarter of

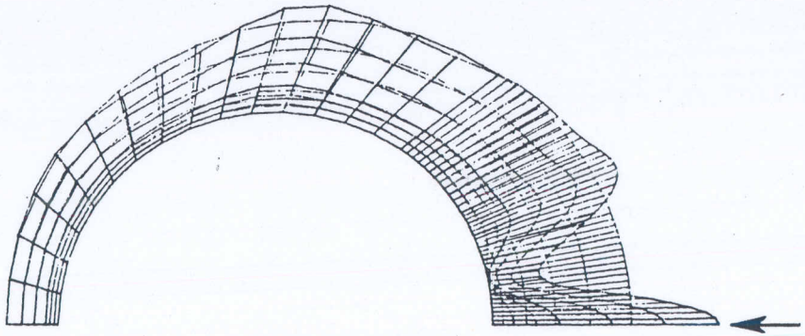

Figure 11: Displacement pattern

the shell near the limit point. A failure mode with one half a wave in the axial direction and a few buckling waves in the circumferential direction, located in the compression zone, is indicated. The post-buckling minimum of the load-deflection diagram (figure 12) is about 60 % of the limit point. The imperfection assumed for the second analysis corresponds to the failure mode of the perfect structure. The maximum imperfection amplitude is 2.5 times the wall thickness. The

load deflection path (figure 12) indicates a reduction of the limit load to 68 % of that for the perfect shell. The postbuckling minima nearly coincide. It should be noted that the example is numerically very sensitive because of the extreme slenderness ratio and the local nature of the failure mechanism. In both cases over 60 steps were necessary.

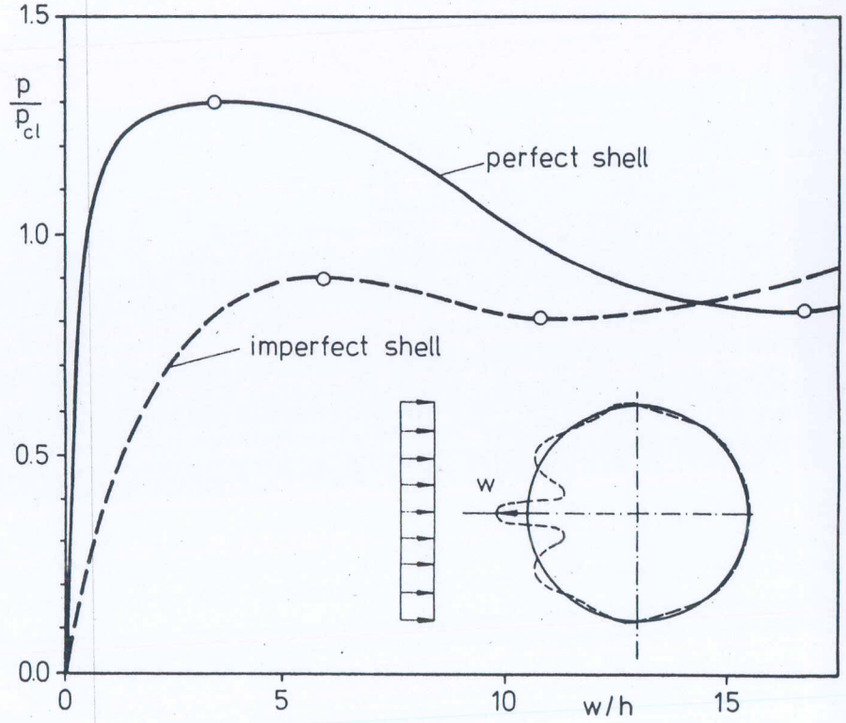

Figure 12: Load - deflection - diagram of a wind loaded shell

6. Conclusions

This study on iterative techniques for passing limit points allows the following conclusions:

* Suppression of equilibrium iterations near the limit point may be a useful procedure but requires very small load steps.
* The method of artificial springs is based on numerical experi-

* The displacement control method requires a proper selection of the controlling parameter. It fails in snap-back situations.

* The constant - arc - length method of Riks/Wempner seems to be the most versatile technique, being advantageous in the entire load range.

Due to modifications of the original method the constraint equation does not need to be solved simultaneously with the equilibrium equations.

Automatic adjustment of the load step and acceleration schemes may further improve the performance. Only minor changes in coding are necessary. Applying the modified Newton-Raphson technique requires the storage of one additional vector. The extra computer time is negligible.

Acknowledgement

The author would like to thank Professor D. W. Murray, University of Edmonton, currently at the University of Stuttgart, for valuable discussions.

References

[1] Riks, E.: The Application of Newton's Method to the Problem of Elastic Stability. J. Appl. Mech. 39 (1972) 1060-1066.

[2] Riks, E.: An Incremental Approach to the Solution of Snapping and Buckling Problems. Int. J. Solids Struct. 15 (1979) 529-551.

[3] Wempner, G. A.: Discrete Approximations Related to Nonlinear Theories of Solids. Int. J. Solids Struct. 7 (1971) 1581-1599.

[4] Bathe, K.-J., Ramm, E., Wilson, E. L.: Finite Element Formulations for Large Deformation Dynamic Analysis. Int. J. Num. Meth. Engng. 9 (1975) 353-386.

[5] Bergan, P. G.: Solution Algorithms for Nonlinear Structural Problems. Int. Conf. on "Engng. Appl. of the F. E. Method", Høvik, Norway 1979, published by A. S. Computas.

[6] Wright, E. W., Gaylord, E. H.: Analysis of Unbraced Multi-Story Steel Rigid Frames. Proc. ASCE, J. Struct. Div. 94 (1968) 1143-1163.

[7] Sharifi, P., Popov, E. P.: Nonlinear Buckling Analysis of Sandwich Arches. Proc. ASCE, J. Engng. Div. 97 (1971) 1397-1412.

[8] Ramm, E.: Geometrisch nichtlineare Elastostatik und finite Elemente. Habilitationsschrift, Universität Stuttgart, 1975.

[9] Argyris, J. H.: Continua and Discontinua. Proc. 1st Conf. "Matrix Meth. Struct. Mech.", Wright-Patterson A. F. B., Ohio 1965, 11-189.

[10] Pian, T. H. H., Tong, P.: Variational Formulation of Finite Displacement Analysis. IUTAM Symp. on "High Speed Computing of Elastic Structures", Liège 1970, 43-63.

[11] Zienkiewicz, O.C.: Incremental Displacement in Non-Linear Analysis. Int. J. Num. Meth. Engng. 3 (1971) 587-588.

[12] Lock, A. C., Sabir, A. B.: Algorithm for Large Deflection Geometrically Nonlinear Plane and Curved Structures. In "Mathematics of Finite Elements and Applications" (ed. J. R. Whiteman), Academic Press, N. Y. 1973, 483-494.

[13] Haisler, W., Stricklin, J., Key, J.: Displacement Incrementation in Nonlinear Structural Analysis by the Self-Correcting Methods. Int. J. Num. Meth. Engng. 11 (1977) 3-10.

[14] Nemat-Nasser, S., Shatoff, H. D.: Numerical Analysis of Pre- and Postcritical Response of Elastic Continua at Finite Strains. Comp. Struct. 3 (1973) 983-999.

[15] Batoz, J.-L., Dhatt, G.: Incremental Displacement Algorithms for Nonlinear Problems. Int. J. Num. Meth. Engng. 14 (1979) 1262-1267.

[16] Wessels, M.: Das statische und dynamische Durchschlagsproblem der imperfekten flachen Kugelschale bei elastischer rotationssymmetrischer Verformung. Dissertation, TU Hannover, 1977, Mitteil. Nr. 23 des Instituts für Statik.

[17] Crisfield, M. A.: A Fast Incremental/Iterative Solution Procedure that Handles "Snap-Through". Proc. Symp. on "Computational Methods in Nonlinear Structural and Solid Mech.", Washington, Oct. 1980.

[18] Brendel, B., Häfner, L., Ramm, E., Sättele, J. M.: Programmdokumentation - Programmsystem NISA. Bericht, Institut für Baustatik, Universität Stuttgart, 1977.

[19] Ramm, E.: A Plate/Shell Element for Large Deflections and Rotations. Symp. "Formulations and Computational Algorithms in F. E. Analysis", Cambridge 1976, MIT Press 1977.

[20] Sabir, A. B., Lock, A. C.: The Application of Finite Elements to the Large Deflection Geometrically Nonlinear Behaviour of Cylindrical Shells. In "Variational Methods in Engng." (ed. C. A. Brebbia and H. Tottenham), Southampton, University Press (1972) 7/66 - 7/75.

[21] Brendel, B., Fischer, D., Ramm, E., Rammerstorfer, F.: Linear and Nonlinear Stability Analysis of Thin Cylindrical Shells under Windloads. To be published, J. Struct. Mech. 1981.

Appendix I: The Artificial Spring Method

According to figure 3 the vector of the total external loads ${}^{i}\mathbf{G}$ of the modified system is decomposed into the real load vector ${}^{i}\mathbf{P}$ and the part resisted by the springs ${}^{i}\mathbf{f}$.

$$ {}^{i}\mathbf{G} = {}^{i}\mathbf{P} + {}^{i}\mathbf{f} \qquad \text{(A 1)} $$

To retain the desired ratio of specified loads it is required that all components of the real load can be obtained by one common "load-reduction-factor" ${}^{i}\gamma$

$$ {}^{i}\mathbf{P} = {}^{i}\gamma \cdot {}^{i}\mathbf{G} \qquad \text{(A 2)} $$

That is, all components of configuration i have the same ratio

$$ \frac{{}^{i}f_k}{{}^{i}G_k} = 1 - {}^{i}\gamma \qquad i = 1,2,3 \cdots n \qquad \text{(A 3)} $$

It follows that springs have to be attached to all loaded degrees-of-freedom and all spring stiffnesses are coupled. The spring stiffness matrix $\mathbf{c}$ is defined by

$$ {}^{i}\mathbf{f} = \mathbf{c} \cdot {}^{i}\mathbf{u} \qquad \text{(A 4)} $$

Energy principles require $\mathbf{c}$ to be a symmetrical matrix ($c_{k\ell} = c_{\ell k}$). Equation (A 3) allows the elements $c_{k\ell}$ of the matrix to be determined if one reference stiffness c_{11} is prescribed

$$ c_{kl} = \frac{{}^{i}G_k \cdot {}^{i}G_l}{({}^{i}G_1)^2} c_{11} \qquad \text{(A 5)} $$

or if the reference load vector $\mathbf{P}$ is introduced

$$ \mathbf{c} = \frac{c_{11}}{P_1^2} \cdot \mathbf{P} \cdot \mathbf{P}^T \qquad \text{(A 6)} $$

The iteration equation, eq. (3 a), is modified to

$$ ({}^{i}\mathbf{K} + \mathbf{c}) \cdot \Delta\mathbf{u}^{(i)} = {}^{i}\mathbf{P} + {}^{i}\mathbf{f} \quad - {}^{i}\mathbf{F} $$

The right hand side expresses the out-of-balance forces. After iteration ($j \rightarrow m+1$) the real loads are determined by eq. (A 2):

$$ {}^{m+1}P = {}^{m+1}\gamma \cdot {}^{m+1}G \qquad \text{with} \quad {}^{m+1}G = {}^{m+1}\lambda \cdot P \qquad \text{(A 8)} $$

The "load-reduction factor" is obtained by eq. (A 3):

$$ {}^{m+1}\gamma = 1 - \frac{c_{11}}{{}^{m+1}\lambda \cdot P_1^2} \; P^T \cdot {}^{m+1}u \qquad \text{(A 9)} $$

It was found that an effective value of c_{11} is one which leads to $0 < {}^{m+1}\gamma < 0.6$ at the beginning of the analysis [7], [8].

Appendix II: Iteration on a "Sphere"

The "sphere" with the center at m and the radius ds of the initial tangent vector $\vec{t}^{(1)}$ (figure 13) is defined by

$$ \vec{r}^{(j)} \cdot \vec{r}^{(j)} - ds^2 = 0 \qquad \text{(A 10)} $$

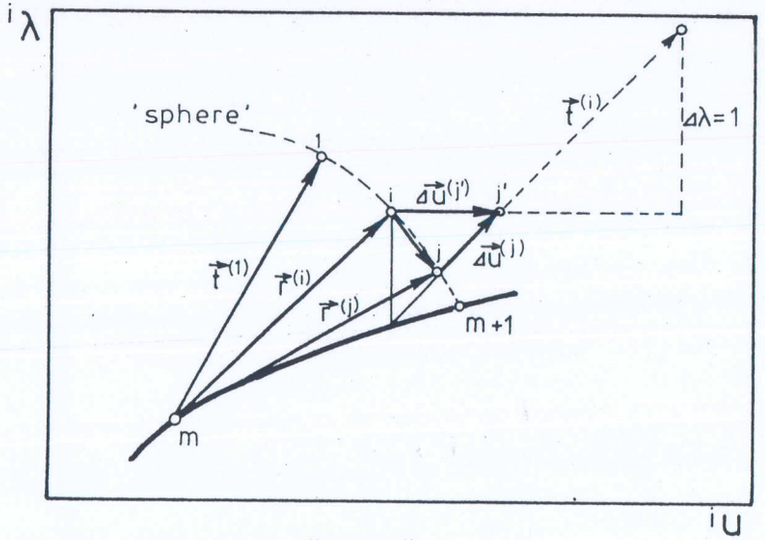

Figure 13: Iteration on a "sphere"

If the radius vector is replaced by

$$ \vec{r}^{(j)} = \vec{r}^{(i)} + \vec{\Delta u}^{(j)} \qquad \text{(A 11)} $$

and eq. (16) is taken into consideration eq. (10) results in

$$ \vec{\Delta u}^{(j)} \cdot (\vec{\Delta u}^{(j)} + 2 \vec{r}^{(i)}) = 0 \qquad \text{(A 12)} $$

or in matrix notation

$$ \Delta u^{(j)T} (\Delta u^{(j)} + 2 \cdot u^{(i)}) + \Delta\lambda^{(j)} (\Delta\lambda^{(j)} + 2 \lambda^{(i)}) = 0 \qquad \text{(A 13)} $$

$\Delta u^{(j)}$ is expressed by eq. (13 a). Then eq. (A 13) leads to a quadratic constraint equation for the load parameter $\Delta\lambda^{(j)}$ which is the equivalent to eq. (19)

$$ a \cdot (\Delta\lambda^{(j)})^2 + 2 b \, \Delta\lambda^{(j)} + c = 0 \qquad \text{(A 14)} $$

with the coefficients

$$ \begin{aligned} a &= 1 + (\Delta u^{(j)II})^T \Delta u^{(j)I} \\ b &= \lambda^{(i)} + (\Delta u^{(j)I})^T (\Delta u^{(j)II} + u^{(i)}) \\ c &= (\Delta u^{(j)II})^T (\Delta u^{(j)II} + 2 \cdot u^{(i)}) \end{aligned} \qquad \text{(A 15)} $$

References.

1. A.B. Sabire, A.C. Lock, "The Application of Finite Elements to the Large Deflection, Geometrically Nonlinear Behavior of Cylindrical Shells", in Variational Methods in Engineering, edited by C.A. Brebbia and H. Tottenbam, Southampton U. Press, 1972.

2. E. Ramm, "Strategies for Tracing the Nonlinear Response near Limit Points", in Nonlinear Finite Element Analysis in Structural Mechanics, edited by W. Wundelich, E. Stein and K.J. Bathe, Springer-Verlag, Berlin, 1981.

3. M.A. Crisfield, "A Fast Incremental/Iterative Solution Procedure That Handles 'Snap-through'", Computers and Structures, Vol. 13, pp 55-62, 1981.